TECHNICAL MEMORANDUMS

NATIONAL ADVISORY COMMITTEE FOR AERONAUTICS

No. 1051

THE COUPLING OF FLEXURAL PROPELLER VIBRATIONS WITH THE TORSIONAL CRANKSHAFT VIBRATIONS

By J. Meyer

Jahrbuch 1938 der deutschen Luftfahrtforschung

Washington
December 1943

NATIONAL ADVISORY COMMITTEE FOR AERONAUTICS

TECHNICAL MEMORANDUM NO. 1051.

THE COUPLING OF FLEXURAL PROPELLER VIBRATIONS WITH THE TORSIONAL CRANKSHAFT VIBRATIONS*

By J. Meyer

The exact mathematical treatment of the problem is possible by replacing the propeller blade by a homogeneous prismatic rod. Conclusions can then be drawn as to the behavior of an actual propeller, since tests on propeller blades have indicated a qualitative agreement with the homogeneous rod. The natural frequencies are determined and the stressing of the systems under the various vibration modes are discussed.

SUMMARY

For the homogeneous prismatic rod assumed equivalent to the propeller blade, the mathematical solution for the coupling of the flexural with the torsional vibrations of an elastic system consisting of a single mass or of several masses is presented, and valid conclusions are derived for the propeller. Extensive tests confirmed the theoretical results.

The most important conclusion derived was that the coincidence of a harmonic with the torsional vibration, since it gives two close-lying natural frequencies of the crankshaft-propeller system is unfavorable, the crankshaft and hub, the propeller blade root, and also the blade itself at the tip being thereby stressed to a dangerous degree. By spreading apart the two frequencies, as can be done by a change in the elasticity of the torsionally vibrating component system, the harmonics in question can be rendered harmless because their position is little affected by a change in the magnitudes of the torsionally vibrating system. The torsional vibration of

---

*"Die Kopplung der Luftschrauben-Biegeschwingungen mit den Kurbelwellen-Drehschwingungen." Jahrbuch 1938 der deutschen Luftfahrtforschung, pp. II 141-159.

the system cannot, however, be eliminated by similar combinations. This can be done only by employing a damper or an elastic hub (reference 17). The maximum vibration moment in the blade root - barring a few exceptions - always acts in the direction of the chord.

OBJECT OF THE INVESTIGATION

In recent years the question as to the cause and prevention of propeller failure in flight has become of greatest importance. The failures are all found to be caused by fatigue stresses due to the flexural vibrations of the propeller blade. A torsiogram of an As-8 engine was of particular interest (fig. 1). The curve shows, instead of a single maximum, two maximums of the sixth order. This phenomenon indicates vibrations of the propeller blade because new degrees of freedom can be added to those of the crankshaft only through the presence of an elastic propeller blade. It may be remarked in passing that in a few cases vibration of the propeller could be established by the naked eye alone. In order to be able to measure experimentally the propeller vibrations occurring in flight, the DVL, since 1934, has been employing the test apparatus shown in figure 2 (reference 17). The setup reproduces the vibrations of the actual radial engine-propeller system. A shaft supported on two bearings and the torsional elasticity of which is of the order of magnitude corresponding to that of most crankshafts carries at one end the propeller with hub to be investigated and at the other end a rotating mass on which two unbalanced weights displaced in the same sense by 180° excite the torsional harmonics, corresponding to the pure vibration torque of the engine. The mass moment of inertia likewise corresponds approximately to that of a large radial engine. With the most usual types of propellers, for rotations of the unbalanced weight up to 10,000 rpm, there were always obtained three frequencies at which the entire system strongly vibrated (table 1). What appears striking in table 1 is that the frequencies of the center column are practically constant while those of the other two are not, and hence depend to a large extent on the given propeller type. The form of the vibration of the second and third frequencies was in most of the cases very similar, although for the second frequency the rotating mass - with few exceptions - underwent considerably larger deflections. The notation

n_1, n_2, and n_D of the columns will be explained. In the course of these investigations the question arose to what extent the flexural propeller vibrations measured on this setup were independent of the coupled torsionally vibrating system.

In the present paper, starting from the differential equation setup for the elastic propeller, the relations holding for the coupling of the flexural propeller vibrations with the torsional crankshaft vibrations are derived.* An explanation is thereby provided for the above-mentioned phenomena. The natural frequencies of the crankshaft-propeller system cannot, however, be numerically determined in this manner. An improved test setup is proposed that can also be used for in-line engines. It is shown, furthermore, that coincidence of the natural frequencies of both component systems, crankshaft and propeller, is particularly dangerous and that the natural frequencies of the entire system and the deflections for equal exciting torque in general depend on the propeller pitch angle.

SETUP OF THE DIFFERENTIAL EQUATION FOR FREE VIBRATION

There is first considered the equivalent system of a radial engine with propeller assumed rigid (fig. 3).

θ_D engine ~~mass~~, kgcms^2 *polar moment of inertia of moving parts of engine*

θ_L propeller ~~mass~~, kgcms^2 *polar moment of inertia of propeller*

c shaft elasticity, kgcm/rad

φ *angular displacement, rad*

W.O'Sullivan 1/24/44

The differential equation for this case is

$$\left.\begin{aligned} \theta_D \ddot{\varphi}_D + c\,(\varphi_D - \varphi_L) &= 0 \\ \theta_L \ddot{\varphi}_L + c\,(\varphi_L - \varphi_D) &= 0 \end{aligned}\right\} \qquad (1)$$

with the solution

$$\omega^2 = c\,\frac{\theta_D + \theta_L}{\theta_D\,\theta_L}$$

or

*At the conclusion of the above investigation there was brought to the attention of the author a paper which likewise takes up the same problem. (See reference 19.)

$$\omega^2 = \frac{c}{\theta_D}\left(1 + \frac{\theta_D}{\theta_L}\right)$$

Actually, however, on account of the elasticity of the propeller blades the crankshaft will not be coupled to a rigid mass but to a vibrating structure with infinite degrees of freedom. The propeller is therefore replaced by an elastic rod which is fixed to a hub, θ_N (fig. 4).

Equilibrium is possible only if the rod, vibrating at position $x = l$, produces a moment the component of which in the plane at right angles to the shaft axis is exactly equal to that acting on the mass θ_N. A rod can vibrate in two mutually perpendicular directions, corresponding to the two principal axes of inertia of its cross section. In the general case if the rod is set oblique to the torsional vibration plane, vibrations about the two principal axes will be excited. If $y(x)$ denotes the deflection, the moment produced about the longer axis (the chord) is $EJ^h_{(l)}y''^h_{(l)}$ and that about the shorter axis $EJ^{f\,l}_{(l)}\ y''^{f\,l}_{(l)}$. Both moments possess a component in the torsional vibration plane. If α denotes the angle which the shorter principal axis of the section makes with the plane of rotation, the differential equation of the system from which the natural frequencies are computed when there are S rods is

$$\left.\begin{aligned}
&\theta_D\,\ddot{\varphi}_D + c(\varphi_D - \varphi_N) = 0\\
&\theta_N\,\ddot{\varphi}_N + c(\varphi_N - \varphi_D)\\
&\qquad = -SE\left\{J^{f\,l}_{(l)}\ y''^{f\,l}_{(l)}\cos\alpha + J^h_{(l)}\ y''^h_{(l)}\sin\alpha\right\}\\
&\qquad E\,\frac{\partial^2}{\partial x^2}\left[J^{f\,l}_{(x)}\,\frac{\partial^2 y^{f\,l}}{\partial y^2}\right] + \mu(x)\,\frac{\partial^2 y^{f\,l}}{\partial t^2} = 0\\
&\qquad E\,\frac{\partial^2}{\partial x^2}\left[J^h_{(x)}\,\frac{\partial^2 y^h}{\partial x^2}\right] + \mu(x)\,\frac{\partial^2 y^h}{\partial t^2} = 0
\end{aligned}\right\} \qquad (2)$$

with the boundary conditions

1. $y'''(0) = 0$ 3. $y'^{fl}_{(l)} = \varphi_N \cos\alpha$; $y'^{h}_{(l)} = \varphi_N \sin\alpha$

2. $y''(0) = 0$ 4. $y^{fl}_{(l)} = r\varphi_N \cos\alpha$; $y^{h}_{(l)} = r\varphi_N \sin\alpha$

and $\mu(x)$ and $J(x)$ may be written $\mu_{(l)}Q(x)$ and $J_{(l)}P(x)$. The function $y(x,t)$, according to Bernoulli, may be written $y(x,t) = y(x) \sin \omega t$. The partial differential equation then goes over into the ordinary linear equation

$$\left.\begin{aligned} \frac{d^2}{dx^2}\left[P^{fl}_{(x)}\,\frac{d^2y^{fl}}{dx^2}\right] - k^4\,Q_{(x)}\,y^{fl}_{(x)} = 0;\quad k^4 = \frac{\mu_{(l)}\omega^2}{EJ^{fl}_{(l)}} \\ \frac{d^2}{dx^2}\left[P^{h}_{(x)}\,\frac{d^2y^{h}}{dx^2}\right] - i^4\,Q_{(x)}\,y^{h}_{(x)} = 0;\quad i^4 = \frac{\mu_{(l)}\omega^2}{EJ^{h}_{(l)}} \end{aligned}\right\} \quad (3)$$

and setting

$$\dot{\varphi}_D = \Phi_D \sin\omega t \quad \text{and} \quad \varphi_N = \Phi_N \sin\omega t$$

the system of equations becomes

$$\left.\begin{aligned} &-\theta_D\,\omega^2\Phi_D + c(\Phi_D - \Phi_N) = 0 \\ &-\Phi_N\,\omega^2\Phi_N + c(\Phi_N - \Phi_D) \\ &\quad = -S\Xi\left\{J^{fl}_{(l)}\,y''^{fl}_{(l)}\cos\alpha + J^{h}_{(l)}\,y''^{h}_{(l)}\sin\alpha\right\} \\ &\left[P^{fl}_{(x)}\,y''^{fl}_{(x)}\right]'' - k^4\,Q_{(x)}\,y^{fl}_{(x)} = 0 \\ &\left[P^{h}_{(x)}\,y''^{h}_{(x)}\right]'' - i^4\,Q_{(x)}\,y^{h}_{(x)} = 0 \end{aligned}\right\} \quad (4)$$

The solution of the problem depends on the solution of the last two differential equations (4). The variation of the functions $J(x)$ and $\mu(x)$ over the propeller length is such, however, that great difficulty is encountered in obtaining the complete solution in exact form. The propeller blades are therefore replaced by homogeneous rods of

rectangular section. For this case the solution can be exactly obtained, and provides information as to the relations for the actual propeller.

SOLUTION FOR THE HOMOGENEOUS ROD

For the prismatic homogeneous rod with $P = Q = 1$ the two differential equations (3) simplify to

$$\left.\begin{aligned} y^{IV\ fl}_{(x)} - k^4\, y^{fl}_{(x)} &= 0 \\ y^{IV\ h}_{(x)} - i^4\, y^{h}_{(x)} &= 0 \end{aligned}\right\} \qquad (5)$$

Taking account of the boundary conditions 1 and 2, there are obtained for $y(x)$ the expressions

$$y^{fl}_{(x)} = A^{fl}\,(\text{Cosh } kx + \cos kx) + B^{fl}\,(\text{Sinh } kx + \sin kx)$$

$$y^{h}_{(x)} = A^{h}\,(\text{Cosh } ix + \cos ix) + B^{h}\,(\text{Sinh } ix + \sin ix)$$

where A and B are constants.

The following brief notation is used for several expressions arising in the computation of $y''_{(l)}$ and satisfying the boundary conditions 3 and 4, where $kl = k'$ and $il = i'$

$$\frac{\text{Sinh } k' \cos k' - \text{Cosh } k' \sin k'}{1 + \text{Cosh } k' \cos k'} = f\,(k')$$

$$\frac{\text{Sinh } k' - \sin k'}{\text{Cosh } k' + \cos k'} = \sigma(k'); \qquad \frac{\text{Cosh } k' - \cos k'}{\text{Cosh } k' + \cos k'} = \tau(k')$$

similarly for i'.

There is then obtained for

$$J^{fl}_{(l)}\, y''^{fl}_{(l)} \cos \alpha + J^{h}_{(l)}\, y''^{h}_{(l)} \sin \alpha$$

the expression

$$J^{f\,l}_{(l)}\ \Phi_N \cos^2\alpha\ \frac{k'}{l}\left\{f(k')\left[1-\frac{r}{l}\,k'\,\sigma(k')\right]+\frac{r}{l}\,k'\,\tau(k')\right\}$$

$$+\ J^{h}_{(l)}\ \Phi_N \sin^2\alpha\ \frac{i'}{l}\left\{f(i')\left[1-\frac{r}{l}\,i'\,\sigma(i')\right]+\frac{r}{l}\,i'\,\tau(i')\right\}$$

The above can be written briefly

$$J^{f\,l}_{(l)}\ \Phi_N \cos^2\alpha\ \frac{k'}{l}\left[G(k')+\frac{J^{h}_{(l)}}{J^{f\,l}_{(l)}}\,\frac{i'}{k'}\tan^2\alpha\ H(i')\right]$$

where $G(k')$ and $H(i')$ denote the generally different functions in the braces.

The expression which is to be set equal to

$$-SE\left\{J^{f\,l}_{(l)}\ y''^{f\,l}_{(l)}\cos\alpha+J^{h}_{(l)}\ y''^{h}_{(l)}\sin\alpha\right\}$$

is

$$\frac{\theta_D\,\theta_N\,\omega^4-c(\theta_D+\theta_N)\,\omega^2}{c-\theta_D\,\omega^2}\,\Phi_N\equiv\frac{1}{f_M}\,\Phi_N$$

Setting $\frac{c}{\theta_D}=\Omega^2$ and $\omega^2=v^2\,k'^4$ where $v^2=\frac{EJ^{f\,l}_{(l)}}{\mu_{(l)}\,l^4}$

there is obtained

$$-\frac{1}{\Phi_N}\,f_M(k')\equiv\frac{1}{\Phi_N}\,\frac{1-\frac{v^2}{\Omega^2}\,k'^4}{v^2\,k'^4\left[\theta_D+\theta_N\left(1-\frac{v^2}{\Omega^2}\,k'^4\right)\right]}$$

Eliminating Φ_N, the solution becomes

$$-SEJ^{f\,l}_{(l)}\,\frac{k'}{l}\,f_M(k')=\frac{1}{\cos^2\alpha\left[G(k')+\frac{J^{h}_{(l)}}{J^{f\,l}_{(l)}}\,\frac{i'}{k'}\tan^2\alpha\ H(i')\right]}$$

or

$$F_M(k') = F_S(k') \tag{6}$$

The expression on the left-hand side is conveniently transformed into

$$F_M(k') \equiv \frac{S\,\mu(l)\,l^3}{\theta_D} \frac{1 - \frac{\nu^2}{\Omega^2} k'^4}{1 + \frac{\theta_N}{\theta_D}\left(1 - \frac{\nu^2}{\Omega^2} k'^4\right)} \frac{1}{k'^3} \tag{7}$$

It remains to replace i' by k' in the expression $F_S(k')$.

$$k^4 = \frac{\mu(l)\,\omega^2}{E J^f(l)} \quad \text{and} \quad i^4 = \frac{\mu(l)\,\omega^2}{E J^h(l)}$$

so that

$$\frac{l}{k} = \sqrt[4]{\frac{J^f(l)}{J^h(l)}}$$

Hence

$$F_S(k') \equiv \frac{1}{\cos^2\alpha\left[G(k') + \sqrt[4]{\frac{J^h(l)}{J^f(l)}}^3 H\left(\sqrt[4]{\frac{J^f(l)}{J^h(l)}}\, k'\right)\tan^2\alpha\right]} \tag{8}$$

Figure 5 shows the function $F_S(k')$ for $\alpha = 0$ and $r = 0$. The points of intersection with the axis of abscissas give the characteristic values k_e' for the rod fixed at $x = l$ with the boundary conditions y'''

$$y'''(0) = y''(0) = 0; \quad y'(l) = y(l) = 0;$$

the values of k' are 1.875, 4.694, 7.855, 10.996, and so forth.

The asymptotic positions 3.927, 7.068, 10.210, and so forth, give the characteristic values k_e' of the rod for the boundary conditions

$$y'''(0) = y''(0) = 0; \quad y''(l) = y(l) = 0$$

Figures 6 and 7 show the function $F_S(k')$ for $\alpha = 0$ and $r = 0.1\,l$ and $0.2\,l$, respectively. While the zero positions of $F_S(k')$ remain the same, the asymptotic positions are displaced. This is explained by the fact that for the frequencies given by the zero positions, the hub is always at rest and therefore plays no part no matter how large r is. The boundary conditions for the rod are the same. For the asymptotic positions one boundary condition was $y(l) = 0$. Actually, however, it is $y(l) = r\Phi_N$. For this reason the asymptotic position must be displaced.

Figures 8 to 13 give the function $F_S(k')$ for $r = 0$ and $\alpha = 0^\circ$, 15°, 30°, 45°, 60°, 90° for a ratio $J^h/J^{f\,l} = 16$. Figures 14 and 15 give the $F_S(k')$ function for $\alpha = 60$ and $r = 0.1\,l$ and $0.2\,l$, respectively.

It may be seen that for the obliquely set rod the two functions $F_S(k')$ for $\alpha = 0^\circ$ and $\alpha = 90^\circ$ are superposed. Since the zero positions remain the same, the various branches of the curve must crowd together. The more one of the two principal vibration directions is turned out of the torsional vibration plane, the more the corresponding curves draw together. Each branch of the $F_S(k)$ curve again runs between two asymptotes. The corresponding value of k' gives for both vibration directions a composite form of vibration such that the bending moment of the rod at the blade root is zero in the torsional vibration plane.

The position of the $F_S(k')$ branches for the vibration about the chord depends on the ratio

$$\sqrt[4]{\frac{J^h_{(l)}}{J^{f\,l}_{(l)}}}$$

For $J^h_{(l)}/J^{f\,l}_{(l)} = 16$ the above ratio is equal to 2. The zero positions are therefore at double the k_e' values of the vibrations about the small axis: that is, 3.750, 9.388, and so forth. From this it may be seen that for the homogeneous prismatic rod fixed at one end, the fundamental vibration about the small axis is followed

directly by the fundamental vibrations about the larger axis, provided the ratio $J^{h}_{(l)}/J^{fl}_{(l)}$ is smaller than $(4.694/1.875)^4 = 39.3$. If the ratio is larger, it means that the fundamental vibration about the longer axis follows only after the first harmonic about the smaller axis. This holds quite generally also for nonhomogeneous rods and hence for propellers except that the ratio $J^{h}_{(l)}/J^{fl}_{(l)}$ and also $G(k')$ and $H(i')$ are different functions.

With each vibration of the rod there is thus associated such a $F_S(k')$ branch - that is, since there are two vibration directions each degree is represented twice. In general, the $F_S(k')$ branch corresponding to the nth degree intersects the k' axis at k_e' and at $\sqrt[4]{J^{h}_{(l)}/J^{fl}_{(l)}}\, k'$ if $G(k')$ and $H(i')$ are equal.

The function $F_S(k')$ is quite independent of the material constants of the rod. It is valid for all rods having $J(x)$ and $\mu(x)$ constant over their length. All constants of the crankshaft-rod system except for the ratio r/l and J_h/J_{fl} are included in the expression for $F_M(k')$. This has the advantage that on varying a constant only one function is varied and the relations are thus more clearly seen.

The engine function possesses a zero and, if $\theta_N \neq 0$, an infinity. The zero - that is, the intersection with the k' axis, gives the natural frequency $\sqrt{c/\theta_D}$ of the torsional component system up to the hub. The infinity gives the natural frequency $\sqrt{c\,\frac{\theta_D + \theta_N}{\theta_D\,\theta_N}}$ of the system: rotating mass - elasticity - mass of hub. The zero position depends only on the ratio ν/Ω. The natural frequencies of the entire system including the rod are obtained from the relation $\omega = \nu\, k'^2$, where the k' are determined by the intersections of the two functions $F_S(k')$ and $F_M(k')$. The validity of these relations was checked with the aid of numerous tests with rectangular section iron rods. Figure 16 shows, attached to the shaft, the hub in which two prismatic homogeneous rods may be inserted at different settings. From the $F_S(k')$-$F_M(k')$ diagram it is clear that through the coupling the natural frequencies (zeros of $F_M(k')$ and $F_S(k')$) of the component systems are displaced.

There will now be determined the natural frequencies of a single-mass system with rectangular rod the constants of which correspond to those of a 700-horsepower radial engine. Let $\theta_D = 10$ cmkgs^2; $S_{ml}{}^2 = 1000$ cmkgs^2; $\Omega = 630 s^{-1}$ (n = 6000 rpm) and in the first case $\theta_N = 0$, and in the second case $\theta_N = \theta_D$.

For each case the functions F_S and F_M are drawn for a blade which corresponds in its dimensions to a large propeller. In the function $F_S(k')$, $J_h/J_{fl} = 16$; $r = 0$; and $\alpha = 60^\circ$. In the function F_M, $\nu = 40$. The first case on figure 17 corresponds to the relations obtaining for an adjustable pitch propeller or for a noncontrollable pitch wood propeller. The second case on figure 18 corresponds to that of controllable pitch propeller for which the mass moment of inertia of the hub may have the same value as that of the engine. There is thus obtained:

	n_1	n_2	n_3 (rpm)	n_4	n_5
Case 1	1530	6100	8400	22,600	
Case 2	1530	6100	8400	19,200	23,600

For comparison there are given the corresponding values that were obtained for a BMW-Electron-controllable-pitch propeller on a test stand similar to that of figure 2: θ_D was equal to 11.7 kgcms^2, $\theta_N = 6$ to 9 cmkgs^2 (estimated), $\Omega = 650 s^{-1}$.

n_1	n_2	n_3 (rpm)	n_4
2000	5600	6100	10,800

The rod in each case possessed the vibration form obtained by substituting the value k' given by the point of intersection in the function $y(x)$. It can only possess its natural vibration form for one end held fixed if a node occurs in the hub and the hub is thus at rest. This is possible for the following values of k':

$$k' = 1.875,\ 4.694,\ 7.855, \text{ and so forth.}$$

The point of intersection of F_M with the k' axis is then always simultaneously the intersection of an F_S branch with the k' axis. It is seen that in these cases the frequency of the entire system cannot vary if

the blades are rotated in the hub – that is, their pitch is varied. In all other cases the natural frequency of the entire system varies. It can only possess the form of vibration corresponding to the condition $y''(l) = 0$ if the infinity of the $F_S(k')$ function coincides with one of the $F_M(k')$ function. All the vibrations over both axes can always be excited as long as neither of the two principal vibration planes lies in the torsional vibration plane. That the previous conclusions hold similarly for propellers is shown by figure 19, which gives the variation with pitch angle of the first three natural frequencies of a single-mass system with rectangular section rod, a BWM controllable pitch propeller, and an As-8 adjustable propeller.

Figures 17 and 18 show further that if the intersection of F_S with the u branch of F_M lies above the k' axis, it means that in the torsional-vibrating system there are $u - 1$ nodes and in the blade there are v nodes where v is the degree of the intersected F_S branch. If the point of intersection lies below the k' axis there are u nodes in the torsional vibrating system and $v - 1$ in the blade.

For practical purposes a knowledge of the first three frequencies is of particular importance, since the others can only be excited by the high harmonics of the torsional-force oscillogram which are very small. For this reason, it is sufficient to consider these first three frequencies alone. Only two kinds of propellers are possible: namely, those to which the fundamental vibration about the chord, on account of the thin hub shaft, lies below the first harmonic about the smaller axis and those for which the reverse is the case. First, case 1 is considered. In figure 20, the first three branches of the $F_S(k')$ function for the prismatic-homogeneous rod are drawn for a ratio $J_h/J_{fl} = 16$ and $\alpha = 60^\circ$, $r = 0$. The corresponding $F_M(k')$ function for $\alpha = 90^\circ$ is also shown dotted. The heavy continuous curves are three $F_M(k')$ functions. The first represents the case where the natural frequency of the torsionally vibrating system is lower than that of the fundamental vibration about the chord of the rod fixed at one end. The second function gives the case where it is equal to the first harmonic about the small axis, and the third the case where it is greater than that of the first harmonic.

There now arises the question as to which of the three frequencies given by the points of intersection corresponds to the so-called crankshaft natural frequency for the case of a rigid propeller – that is, the frequency causing the strong deflections recorded by the torsiograph of the torsionally vibrating system. It is clear that only one intersection comes into consideration: namely, that which lies very near the intersection of the $F_M(k')$ curve with the k' axis. This fact, however, is not by itself sufficient; since this vibration must also exist for the propeller setting $\alpha = 90^\circ$. The propeller is then most rigid in the direction of the torsional vibration and the vibrations about the small axis are, as it were, uncoupled. The case now corresponds to the rigid propeller.

The case where the prismatic rod is assumed as rigid with regard to vibration about the chord is that for which $J_{h(l)} = \infty$. In this case the rod function $F_S(k')$ is practically of the same shape as the dotted curve on figure 20 with the exception, however, that it always remains below the the k' axis which it intersects at infinity – that is, that the k' axis is an asymptote. It follows from this that the point of intersection corresponding to the torsional vibration also occurs for $\alpha = 90^\circ$ and the branch of the rod function intersected by the engine function $F_M(k')$ must pass continuously into the dotted curve with increasing α. In figure 20, the so-called crankshaft natural frequency is given in the first two cases by the second point of intersection and in the third case by the third point of intersection.

Figure 21 shows the case where the frequency of the fundamental vibration about the chord is greater than that of the first harmonic about the small axis. The ratio $J_h/J_{fl} = 81$ and again $\alpha = 60^\circ$, $r = 0$. From what was said previously, there is similarly obtained the so-called crankshaft natural frequency for the first $F_M(k')$ function from the second point of intersection and, for the second and third functions, from the third point of intersection.

Of the three frequencies considered, one is thus uniquely determined as the natural frequency of the crankshaft with elastic propeller and it is seen that the other two points of intersection lie very close to the k' values for the fundamental vibration and first harmonic about the small axis of the rod fixed at one end. From all this, it follows that for high angles α the three possible

natural frequencies of the system lie very close to the natural frequencies of the two component rod and crankshaft systems when the rod is fixed at the hub. One of the natural frequencies of the system may therefore be denoted as the crankshaft torsional vibration n_D and the two others as fundamental and first harmonic of the rod or propeller n_1 and n_2. This explains the notation of table 1 and the slight variation in the frequency in the second column as compared with the variations of the first and third.

It is seen on figures 17, 18, 20, and 21 that the first harmonic is least shifted by the coupling. The torsional vibration of the system can undergo a relatively large displacement. It may be seen from the expression for the engine function (equation (7))that for equal ratio ν/Ω it intersects the k' axis at a larger angle the smaller the rotation mass θ_D. It follows from this that for a given propeller and given ratio ν/Ω the natural crankshaft frequency of the entire system deviates more from the natural frequency of the torsionally vibrating system the greater the rotating mass θ_D. In the case of the rigid assumed propeller, the corresponding expression for the torsional natural frequency is

$$\omega^2 = \Omega^2\left(1 + \frac{\theta_D}{\theta_L}\right)$$

In practice only propellers generally are used for which the relations are such as are expressed by the function $F_S(k')$ in figure 20. Fundamentally, the first and second engine functions hold for the case when the first harmonic about the small axis is greater than the torsional vibration and the third engine function for the case given in table 1 for the second and fifth propeller, where the first harmonic of the small axis is lower than the torsional vibration of the system.

It is also seen now how the torsional vibration curve of figure 1 is possible. One maximum arises from the crankshaft vibration, the other from the first harmonic. Thus, the explanation, that only by the coincidence of the frequency of the crankshaft torsional vibration with the first harmonic of the propeller does the first one split into two coupling frequencies similar to the resonance pendulum, is untenable. These two resonance positions, according to the foregoing, are always present. Why such

characteristic is so rarely measured, and why the vibration form of the propeller for the second and third frequencies of table 1 may be similar, will be shown later. Furthermore, the torsional vibration frequency in adjusting the blade to high pitch angles must drop because the blade is then set more and more with the wide side in the torsional vibration direction and thus becomes less rigid. In order to see this, consider figure 20. High pitch means here that $\alpha \rightarrow 0$. For the engine function III and II there actually is obtained a lowering of the torsional vibration frequency. Similarly, for the engine function I in the case drawn where the natural frequency Ω of the torsionally vibrating system is greater than that of the blade about the chord ($k_e' = 3.750$). If the engine function I, however, would cut the k' axis ahead of $k_e' = 3.750$ the torsional vibration frequency would rise in setting the blade to a high pitch angle, according to the rule established here, that all natural frequencies of the entire system with increasing uncoupling of the torsional with the flexural vibrations are displaced toward the natural frequency of the blade vibration which is uncoupled. (See fig. 19, As-8 propeller.)

It will now be shown further how the solution (6) goes over into that for the rigid rod as ν approaches infinity. This does not show up in the $F_M(k')$ to $F_S(k')$ diagrams. The greater the value of ν the steeper the function $F_M(k')$ for constant Ω, and its point of intersection with the k' axis lies always more to the left at small k' values. For the rigid rod ($\nu = \infty$) it would lie at $k' = \sqrt{\omega/\nu} = 0$ and the natural frequencies would assume the indeterminate form $\omega = 0 \times \infty$ although ω obviously can still possess also a finite value. The limit must therefore be obtained from the formulas. For this purpose the solution (6) is written

$$F_M(k')\, k'^3 = F_S(k')\, k'^3$$

In this way, in the expression on the right, only k' occurs and on the left, only the product $\nu k'^2$, which may be set equal to ω. There is then obtained

$$F_M(k')\, k'^3 = \frac{S_\mu(l)\, l^3}{\theta_D} \frac{1 - \frac{\omega^2}{\Omega^2}}{1 + \frac{\theta_N}{\theta_D}\left(1 - \frac{\omega^2}{\Omega^2}\right)}$$

and setting for simplification, $\alpha = 0$, $r = 0$

$$F_S(k')\,k'^3 = \frac{2\,k'^3}{\text{Sinh } k' \cos k' - \text{Cosh } k' \sin k'}$$

When ν approaches infinity k' will approach zero, and it is only necessary to investigate the expression for the rod function. The latter is indeterminate. If the denominator, however, is expanded into a series, then

$$F_S(k')\,k'^3 = \frac{2\,k'^3}{\left(k' - \frac{2}{3!}k'^3 - \frac{4}{5!}k'^5 + \ldots\right) - \left(k' + \frac{2}{3!}k'^3 - \frac{4}{5!}k'^5 - \ldots\right)}$$

and for $k' = 0$, the value of the fraction becomes equal to -3. The solution for $\nu = \infty$ then becomes

$$F_M(k')\,k'^3 = -3$$

In solving for ω, the following equation is then obtained

$$\left(\frac{S_\mu(l)\,l^3}{3} + \theta_N\right)\left(1 - \frac{\omega^2}{\Omega^2}\right) = -\theta_D$$

The expression in the first parentheses is no other, however, than the mass moment of inertia – referred to the shaft – of a "propeller" consisting of a prismatic infinitely rigid rod and may be set equal to θ_L. Then

$$\frac{S_\mu(l)\,l^3}{3} + \theta_N = \theta_L$$

$$\theta_L\,(\omega^2 - \Omega^2) = \theta_D\,\Omega^2$$

$$\omega^2 = \Omega^2\left(1 + \frac{\theta_D}{\theta_L}\right)$$

SOLUTION FOR NONHOMOGENEOUS RODS

Having discussed the prismatic homogeneous rod, there will now be investigated how far the computation may be carried through for the nonhomogeneous rod. Start from equation (3) and write

$$P_{(x)}\, y^{IV}_{(x)} + 2P'_{(x)}\, y'''_{(x)} + P''_{(x)}\, y''_{(x)} - k^4 Q_{(x)}\, y_{(x)} = 0$$

The difficulty of solution of this differential equation increases with the complexity of the functions $P(x)$ and $Q(x)$. For this reason there will be set for $P(x)$ and $Q(x)$ the simplest, yet still reasonable exponential expressions, $P(x) = \left(\frac{x}{l}\right)^p$ and $Q(x) = \left(\frac{x}{l}\right)^q$. Dividing the equation by $P(x)$ and setting $p + \epsilon = q$, there is obtained

$$y^{IV}_{(x)} + 2p\,\frac{y'''(x)}{x} + (p^2 - p)\,\frac{y''(x)}{x^2} - \frac{k^4}{l^\epsilon}\, x^\epsilon\, y_{(x)} = 0$$

In the above differential equation p can take any values from $-\infty$ to $+\infty$. For $+\infty > \epsilon \geq -4$ it is a Fuchs-type differential equation and as such is integrable by means of series. Solutions defined at $x = 0$ are obtained only if the i coefficient in a differential equation of the form

$$y^{IV}_{(x)} + R_1\, y'''_{(x)} + R_2\, y''_{(x)} + R_3\, y'_{(x)} + R_4\, y_{(x)} = 0$$

has a pole of, at most, the i^{th} order. If $\epsilon < -4$ then $x = 0$ is a so-called essentially singular point, and for this case there is as yet no complete theory. (See L. Bierberbach, Differentialgleichungn, pp. 195–196.) At any rate, no solutions can then be found in the form of convergent series. Thus, the cases are restricted to $\infty > \epsilon \geq -4$. Since the case $\epsilon = -4$ is solved by setting $y(x) = x^\rho$ the method of series development starts with $\epsilon = -3$. Since only in the cases with $\epsilon \geq -3$ not all four particular integrals involve logarithms, of which use cannot be made, the solution of the differential equation is restricted for $+\infty > p > -\infty$ and $\infty > \epsilon \geq -3$.

Setting $y(x) = \sum_{\nu}^{\infty} a_\nu x^{\rho+\nu}$, there is obtained, since a_o is not to vanish, the "characteristic equation"

$$\rho(\rho - 1)\left\{p^2 + p\left[2(\rho - 2) - 1\right] + (\rho - 2)(\rho - 3)\right\} = 0$$

The above equation has the four roots

$$\rho_1 = 0; \quad \rho_2 = 1; \quad \rho_3 = \frac{5 - 2p}{2} - \frac{1}{2}; \quad \rho_4 = \frac{5 - 2p}{2} + \frac{1}{2}$$

Since ρ_3 and ρ_4 for the various values of p are either equal to ρ_1 and ρ_2 or differ from them by an integer, the corresponding particular integrals involve logarithms and drop out for our case where $y'''(0) = y''(0) = 0$. The first two solutions are found to be

$$y(x) = a_0\psi_0\left[\left(\frac{k^4}{l^\epsilon}\right)^{\frac{1}{4+\epsilon}} x\right] + a_1 \psi_1\left[\left(\frac{k^4}{l^\epsilon}\right)^{\frac{1}{4+\epsilon}} x\right]$$

$$\psi_0 = 1 + \sum_{m=1}^{\infty} \frac{\left[\left(\frac{k^4}{l^\epsilon}\right)^{\frac{1}{4+\epsilon}} x\right]^{(4+\epsilon)m}}{(4+\epsilon)^m\, m!\, P_1^m[(4+\epsilon)m-1]\, P_1^m\left(p^2 + p\left\{2[(4+\epsilon)m-2]-1\right\} + [(4+\epsilon)m-2][(4+\epsilon)m-3]\right)}$$

$$\psi_1 = \left(\frac{k^4}{l^\epsilon}\right)^{\frac{1}{4+\epsilon}} x + \sum_{m=1}^{\infty} \frac{\left[\left(\frac{k^4}{l^\epsilon}\right)^{\frac{1}{4+\epsilon}} x\right]^{(4+\epsilon)m+1}}{(4+\epsilon)^m\, m!\, P_1^m[(4+\epsilon)m+1]\, P_1^m\left(p^2 + p\left\{2[(4+\epsilon)m-1]-1\right\} + [(4+\epsilon)m-1][(4+\epsilon)m-2]\right)}$$

Figure 25 shows the $F_S(k')$ curve for the fundamental vibration $\alpha = 0$ and $r = 0$. Although five terms of the power series were taken, it was not possible to compute exactly the second zero position; because for higher values of k' the computation becomes too inaccurate on account of the rapidly increasing large numbers. The value must lie between 5.2 and 5.4. The first zero position is obtained as 2.67. The corresponding experimental setup is shown on figure 26.

The first zero position for nonhomogeneous rods can easily be found by the Rayleigh method,

$$\omega^2 \leq \frac{E\,J_{(l)}}{\mu_{(l)}} \frac{\int_0^l P_{(x)}\, y''^2_{(x)}\, dx}{\int_0^l Q_{(x)}\, y_{(x)}^2\, dx}$$

$$y(x) = x^4 + ax^3 + bx^2 + cx + d$$

With the boundary conditions

$$y'''(0) = y''(0) = 0;\ y'(l) = y(l) = 0$$

$y(x)$ becomes $y(x) = x^4 - 4\,l^3\,x + 3\,l^4$. There are thus obtained the first zeros for the following five cases:

q	p	ϵ	k_e'	Error (percent)
0	0	0	1.880	0.27
1	1	0	2.69	.75
1	2	−1	2.59	
1	4	−3	2.45	
1	6	−5	2.31	

It is seen that the first zero for propellers must lie in the neighborhood of 2. By the Rayleigh method it is also possible to approximate very closely the functions $\mu(x)$ and $J(x)$ by suitable polynomials of x instead of the simple expression x^p or x^q so that the first zeros can almost accurately be obtained, as the positive error shows for 1.880 as compared with the accurate error value 1.875. Unfortunately, nothing has been gained thereby

for the problem under consideration; since from all that has been said it is not practically possible to compute beforehand the natural frequencies of a torsional-flexural system as was done for the homogeneous prismatic rod. The only magnitudes that can be accurately determined are θ_D and c; θ_N and r/l are no longer uniquely determined. For the longer and shorter axis $\psi_0(x)$ and $\psi_1(x)$, respectively, can be found only approximately, and the function $F_S(k')$ can be practically computed only for the fundamental vibration, which is not of great interest. There is the further difficulty that the angle α on account of the twist cannot be accurately defined. For relations such as those holding for engine function I on figure 20, the angle $\alpha = 0$ also can be defined as that for which the frequency of the first harmonic is a minimum and for the fundamental vibration a maximum. A corresponding consideration holds also for the still higher harmonics. This angle in practice, however, deviates from zero, as tests have shown (see p.26) and has different values for the different vibrations. The deviation from zero may be as much as 30°. This necessarily leads to the direct measurement of the natural frequency of the crankshaft-propeller system. The test setup, however, must permit a variation of the elasticity and the moment of inertia of the rotating mass in order that the corresponding engine may be simulated with sufficient accuracy.

MEASUREMENT OF A PROPELLER

In order to be able to satisfy the condition of accurate simulation of the engine under consideration, the test setup was constructed as shown in figures 27a,b. A rotating mass to which is screwed the unbalanced exciter weight is displaceable on a steel shaft 120 centimeters long and can be held in place by a pressure seat. The mass moment of inertia can be varied by screwing on iron plates, each of 1.1 $kgcms^2$ moment of inertia in steps of 2.4 to 15 $kgcms^2$. With the aid of this apparatus, it is possible to determine, experimentally, the unknown function F_S for the range of practical importance. There is first determined the value ν for the propeller under consideration. For this purpose there is taken in the neighborhood of the blade root a cross section, which is typical of the remainder of the blade (fig. 28).

There is now drawn through the k' axis a family of $F_M(k')$ curves by varying θ_D and c. Each time the corresponding value of θ_D and c is adjusted on the test stand and the frequency ω measured. Then, for each $k' = \sqrt{\frac{\omega}{v}}$ on the corresponding $F_M(k')$ curve a point is marked. The line joining all these points gives a portion of the unknown propeller function $F_S(k')$ not not computable in advance.

This procedure was carried out for a Ju PAK-dural adjustable propeller for the BMW "Hornet" engine. The blade length was chosen $l = 110$ centimeters and the blade width was then obtained as $b = 25$ centimeters and blade thickness $h = 5.7$ centimeters. The ratio J_h/J_{fl} at the position $x = l$ was 16.3. The magnitude of v was computed to be approximately 70, and the value $S\mu(l)l^3$, 743 kgcms^2. The mass moment of inertia of the hub with blade root was 4.93; r/l was approximately 0.15. On figure 29 the various engine functions

$$F_M(k') = \frac{743}{\theta_D} \frac{1 - \frac{4900}{\Omega^2} k'^4}{1 + \frac{4.93}{\theta_D}\left(1 - \frac{4900}{\Omega^2} k'^4\right)} \frac{1}{k'^3}$$

are denoted by the letters a to k. On table 2 the values of θ_D and Ω^2 are given for each of the 10 $F_M(k')$ functions which were adjusted on the test stand. On figure 29 the similarity may be seen of the propeller functions determined by this test with those of the homogeneous prismatic rod on figure 14. It is to be noted that in the latter figure the scale of abscissas was smaller. For the Ju PAK propeller the different harmonics follow each other more rapidly than for the homogeneous rod. There were obtained the values $n_1 = 2800$, $n_2 = 7300$, $n_3 = 13{,}200$ rpm. For the BMW Electron controllable propeller used for comparison, there was obtained $n_1 = 2000$, $n_2 = 6100$, $n_3 = 10{,}800$ rpm.

The test showed that the first harmonic is practically independent of the torsionally vibrating system. For this reason it might be computed in advance if it were sufficient to compute the frequency of the blade fixed at the root, as is possible with the aid of energy methods (references 4 and 5). The assumed rigid end condition at the

root, however, does not actually occur and the degree of fixing, which can be different for each hub, greatly affects the frequency. The effect of the twist which tends to increase the frequency must also be taken into account (reference 8). For this reason, the experimental method is preferred, which enables the simple and accurate determination of the required frequency.

In this connection there will also be considered the factors that affect the first characteristic value k_e' of propellers. For the Ju PAK propellers for a value of ν of 70, this value of k_e' lies at 2.06. For the previously mentioned BMW propeller for a value of ν of 50, it lies at 2.05; and for the As-8 propeller of figure 19 for $\nu = 70$, it lies at 1.93. The characteristic values k_e' for known natural frequency depend on the choice of the magnitude ν and the latter again on the choice of the position $x = l$. The change in the value of ν is very marked only where the blade passes over into the cylindrical shaft, where ν increases very strongly. At a distance of 10 centimeters along the blade, however, it is already only slightly affected by a change in l. The blade naturally can be considered also as extending to the point of attachment. This, in the case of the Ju PAK propeller, would lead to a value of $\nu = 88$ and the k_e' values all would be smaller by 11.2 percent. The $F_S(k')$ function then also must change a little but, on the whole, will be very similar. The k' values would then depend, however, only on the form of the section at the position of attachment — that is, with a thicker shaft the blade would have much lower characteristic values. This, however, is physically unreasonable. Hence the shaft must be considered as belonging to the fixation and not as a part of the elasticity determining the natural frequencies of the blade. For this reason the $F_S(k')$ function for the Ju PAK propeller was determined for the value $\nu = 70$.

EFFECT OF THE CENTRIFUGAL FORCE

A test setup of the kind described above gives only the natural frequencies of the system for the case of a nonrotating propeller. There also must be taken into account, therefore, the increase in the stiffness and hence the natural frequency of the blade as a result of

the centrifugal force in rotation. The increase in the natural frequencies by the centrifugal force of propeller blade fixed at the root is given by Liebers (references 4 and 12) as follows: If $\bar{\omega}$ is the natural frequency for the propeller at rest and ω_u the number of rotations, then for the first three natural frequencies there hold the relations:

$$\omega_1^2 = \bar{\omega}_1^2 + 1.45\ \omega_u^2, \quad \text{fundamental vibration}$$

$$\omega_2^2 = \bar{\omega}_2^2 + 4.40\ \omega_u^2, \quad \text{first harmonic}$$

$$\omega_3^2 = \bar{\omega}_3^2 + 9.20\ \omega_3^2, \quad \text{second harmonic}$$

It is thus a matter of simply adding to the test values obtained, if the latter are practically identical with $\bar{\omega}_1$ and $\bar{\omega}_2$ as can be shown to be the case with the above described apparatus. On account of the large setting angles of the propellers there cannot occur a greater deviation of the frequencies of the fundamental and first harmonic from $\bar{\omega}_1$ and $\bar{\omega}_2$, respectively.

Since the value of ν remains the same under the action of the centrifugal force, the engine function does not change, but the zero positions of the $F_S(k')$ branches lie at higher values of k'. For a speed of $n = 1910$ — that is, $\omega_u = 200$, the increments are

$$\omega_1^2 = \bar{\omega}_1^2 + 58{,}000$$

$$\omega_2^2 = \bar{\omega}_2^2 + 176{,}000$$

If, on the average, $\bar{\omega}_1$ is taken to be 200 and 600, respectively, (chord) and $\bar{\omega}_2 = 700$, then $\omega_1 = 313$ and 647, respectively, (chord) and $\omega_2 = 816$. This is 56.5 and 7.85 percent for ω_1 and 16.6 percent for ω_2. Expressed in terms of k' the increase in the fundamental vibration over the chord is only 25.4 compared to 24.5 which is 3.67 percent. The intersection of the $F_S(k')$ function corresponding to $k' = 3.750$ in figure 20 and $k' = 5.625$ in figure 21 is shifted to the right by about 4 percent. It is easily seen that the frequency of the torsional natural vibration of the entire system is practically not shifted.

SOLUTION FOR A SEVERAL-MASS SYSTEM

There is still to be investigated how the natural frequencies are determined for an in-line engine which can be represented only by a several-mass system.

Let the system consist of 6 masses - corresponding in their dimensions approximately to the BMW-IV engine.

$$\theta_{1-6} = 0.5 \text{ kgcms}^2$$

$$c_{1-5} = 4 \times 10^6 \text{ kgcm/rad}$$

$$c_6 = 2.66 \times 10^6 \text{ kgcm/rad}$$

The first three natural frequencies of this system then lie at

$$\Omega_1 = 635 \qquad \Omega_2 = 1895 \qquad \Omega_3 = 3100$$

In order to simplify the computation, somewhat, each pair of masses is combined into one (fig. 30) so that

$$\theta_{1-3} = 1 \text{ kgcms}^2$$

$$c_{1-3} = 2 \times 10^6 \text{ kgcm/rad}$$

The first three natural frequencies are then computed from the equation

$$\omega^6 - 10^7 \times \omega^4 + 24 \times 10^{12} \times \omega^2 - 8 \times 10^{18} = 0$$

$\Omega_1 = 630$ compared with 635 - 0.8 percent

$\Omega_2 = 1750$ compared with 1895 - 7.7 percent

$\Omega_3 = 2550$ compared with 3100 - 17.8 percent

This deviation is of no significance for our investigation and is given only as a matter of interest. Now consider

the three-mass system. The other magnitudes in the $F_M(k')$ function are assumed to be

$$\left.\begin{aligned} \nu &= 30 \\ S\,\mu_{(l)}\,l^3 &= 1200 \end{aligned}\right\}$$ which values hold for very large propellers.

The function $F_M(k')$ will now be computed for two cases. In the first case $\theta_N = 0$ and in the second case $\theta_N = \Sigma\,\theta_i$ (fig. 31). It can be given, in general, for an arbitrary number of masses if the method of Tolle is used. This method serves to compute the natural frequencies of a several-mass system. If M denotes the moment and a the deflection of any mass, then

$$M_{i,i+1} = M_{i-1,i} - \theta_i\,\omega^2\,a_i$$

$$a_{i+1} = a_i + \frac{M_{i,i+1}}{c_{i,i+1}}$$

Thus starting at the end mass

$$a_1 = 1$$

$$M_{12} = -\theta_1\,\omega^2$$

$$a_2 = 1 - \frac{\theta_1\,\omega^2}{c_{12}}$$

$$M_{23} = M_{12} - \theta_2\,\omega^2\,a_2, \quad \text{and so forth.}$$

If, however, all a_i are expressed by a_1 and all $M_{i,i+1}$ by M_{12} expressions of terms with increasing power of the natural frequency are obtained

$$a_1 = 1$$

$$M_{12} = -\theta_1 \omega^2$$

$$a_2 = 1 - \frac{\theta_1 \omega^2}{c_{12}}$$

$$M_{23} = -\omega^2(\theta_1 + \theta_2) + \omega^4 \frac{\theta_1 \theta_2}{c_{12}}$$

$$a_3 = 1 - \omega^2\left[\theta_1\left(\frac{1}{c_{12}} + \frac{1}{c_{23}}\right) + \theta_2 \frac{1}{c_{23}}\right] + \omega^4 \frac{\theta_1 \theta_2}{c_{12}c_{23}}$$

$$M_{31} = -$$

The function for an n mass system may then be written as

$$F_M(k') = -\frac{S\,\mu(l)\,l^3}{k'^3} \frac{a_n}{M_{n,n+1}} \omega^2$$

where $a_n = 0$ gives the zeros and $M_{n,n+1} = 0$ the infinities of the functions. There are obtained the values:

Case I	First zero	$\Omega_1 = 630$	$k' = 4.58$
	First infinity	$\omega = 1420$	$k' = 6.88$
	Second zero	$\Omega_2 = 1750$	$k' = 7.65$
	Second infinity	$\omega = 2450$	$k' = 9.05$
	Third zero	$\Omega_3 = 2550$	$k' = 9.23$
Case II	First zero	$\Omega_1 = 630$	$k' = 4.58$
	First infinity	$\omega = 848$	$k' = 5.32$
	Second zero	$\Omega_2 = 1750$	$k' = 7.65$
	Second infinity	$\omega = 1845$	$k' = 7.85$
	Third zero	$\Omega_3 = 2550$	$k' = 9.23$
	Third infinity	$\omega = 2580$	$k' = 9.30$

Figures 32 and 33 show the variation of the F_M function (continuous curve). The three masses were now combined into one and the elasticity so chosen that the natural

frequency of this torsionally vibrating system was equal to the first of the three-mass system:

$$c = 3\,\Omega_1^2$$

The substitute function for the first case is then obtained

$$F_M(k') = \frac{400}{k'^3}\left(1 - 2.27 \times 10^{-3}\, k'^4\right)$$

and for the second case

$$F_M(k') = \frac{400}{k'^3}\,\frac{1 - 2.27 \times 10^{-3}\, k'^4}{2 - 2.27 \times 10^{-3}\, k'^4}$$

$$k'_{(F_M=0)} = 4.58; \qquad k'_{(F_M=\infty)} = 5.45$$

Since the substitute function first begins to deviate from that of the three-mass function only at a rather great distance from the k' axis, where the F_S curve runs practically vertical, no difference in the values of k' given by the intersections can occur up to about $k' = 6$. Since the first zero is at 4.58, it means that the equivalent system correctly gives another natural frequency, which lies higher than the first natural frequency of the system Ω_1 by $\frac{6^2 - 4.58^2}{4.58^2} \times 100 = 71.5$ percent — or in round numbers — 70 percent. Thus the higher frequency should be not much greater than

$$\begin{aligned} n &= 6{,}800 \text{ if } n_D = 4{,}000 \\ n &= 10{,}200 \text{ if } n_D = 6{,}000 \\ n &= 17{,}000 \text{ if } n_D = 10{,}000 \end{aligned}$$

If the difference is greater then, having determined the $F_S(k')$ function on the test stand, the engine function is accurately computed or, at least, replaced by the one-, two-, or three-mass system and then made to intersect with the $F_S(k')$ function.

This concludes the investigation of the problem of the coupling of the flexural propeller vibrations with the torsional crankshaft vibrations and the determination of the critical engine speeds. In the following there will be further considered the fundamental stress problems.

THE VIBRATION STRESSES IN THE SYSTEM

A. Theoretical Considerations

In the function $F_S(k')$ zeros are followed by infinities. For the vibrations corresponding to the latter there hold simultaneously the three boundary conditions

$$y'''(0) = 0, \quad y''(0) = 0, \quad y(l) = r\,\Phi_N$$

The fourth condition, corresponding to the zeros, is $y'(l) = 0$. For our system this means that the hub is at rest and the greatest bending moment is at the blade root. In these cases the propeller blade vibrates mainly about one of the two principal moment-of-inertia axes of the cross section. Without twist a rod or propeller blade would vibrate about one of the principal axes only. The entire system vibrates with the frequency $\omega = \Omega$, the rotating mass undergoes relatively the greatest displacements and the component of the largest bending moment of the rod in the torsional vibration plane amounts to

$$\theta_D\,\omega^2\,\Phi_D = c\,\Phi_D$$

The torsional component system is in resonance. As a result of the twist torsional vibrations of the blades may be excited, but these vibrations will not here be considered. It may be remarked in passing that they have, up to the present, been very rarely observed. At the frequency corresponding to $k' = 2.97$ in figure 29, the propeller blade would thus vibrate in its fundamental mode about the chord and at the frequency corresponding to $k' = 3.3$ in its first harmonic about the small axis. To the right and left of each zero of the $F_S(k')$ function the moment at the blade root again decreases, the maximum moment however no longer lying in the direction of one of one of the principal moment-of-inertia axes of the cross section, since a moment now arises about the other axis. In addition to the frequencies corresponding to the zeros,

vibration of the rod occur simultaneously over the two axes and the two moments in these directions together give a resultant moment M which makes an angle β with the torsional vibration plane (fig. 34). This resultant moment must be decomposed into two perpendicular components, one of which acts as a pure bending moment M_B on the shaft. On account of the symmetry in the case of several blades, these bending moments balance each other out, but the shaft is acted on by a tensile or compressive force through which axial vibrations of the crankshaft may be excited (fig. 35). The other component M_D just balances the torsional vibration moment in the shaft. It follows that, since the torsiograph measures only this one component that the moment in the hub is to be assumed considerably higher.

For the vibrations of the rod corresponding to the infinities the fourth boundary condition is $y''(l) = 0$. In this case the bending moment at the blade root is equal to zero and the hub is in motion. These vibration modes can then only arise if the two infinities of the $F_S(k')$ and $F_M(k')$ functions coincide. This is possible if the mass moment of inertia of the hub is not equal to zero. The frequency of this vibration is given by

$$\omega = \sqrt{c \frac{\theta_D + \theta_N}{\theta_D \theta_N}}$$

and the angular displacement of the hub has its maximum value. The maximum occurring bending moment then lies within the propeller blade. All the blades would then be, as it were, in equilibrium; and the rotating mass would only have to balance the moment due to the vibrating hub. Since

$$\theta_D \omega^2 \Phi_D = \theta_N \omega^2 \Phi_N$$

for the displacement of the rotating mass, there is obtained

$$\Phi_D = \Phi_N \frac{\theta_N}{\theta_D}$$

which therefore decreases for given hub displacement as the ratio of the hub mass to the rotating mass. The hub displacement, however, cannot become large, for

$$\Phi_N = \sqrt{y'^{h^2}_{(l)} + y'^{f\,l^2}_{(l)}}$$

On account of the setting angle α, $y'^{h}_{(l)}$ contributes most to the angle Φ_N. For $\alpha = 45^\circ$, $y'^{h}_{(l)} = y'^{f\,l}_{(l)}$; but $y'^{h}_{(l)}$ $(\alpha = 90^\circ)$ is small compared to $y'^{f\,l}_{(l)}$ $(\alpha = 0^\circ)$ since $J^{h}_{(l)}$ also at the blade root is much larger than $J^{f\,l}_{(l)}$. Moreover, $y'^{h}_{(l)}$ must become smaller the more the resonance-indicating value of k', for the prismatic homogeneous rod here considered, differs - for example, from $k' = 7.853$. Hence Φ_N for the vibrations corresponding to the infinity positions is small making Φ_D also small, since the ratio θ_N/θ_D is generally smaller than 1. This holds, also, approximately for the cases where the point of intersection of $F_M(k')$ with $F_S(k')$ which point determines the resonance frequency of the system lies far from the k' axis and there is a node in the shaft. These points of intersection always lie below the k' axis.

The displacements of the rotating mass for the vibrations, the corresponding point of intersection of which lies above the k' axis, are much greater than Φ_N and there is no node in the shaft.

The position of the point of intersection of the engine and rod functions determines not only a resonance frequency of the crankshaft-propeller system but its distance from the k' axis is at the same time a measure of the moment arising in the hub, because the magnitude $F_M(k') = F_S(k')$ represents the reciprocal value of the component of the moment at the hub divided by

$$SEJ^{f\,l}_{(l)} \frac{k'}{l} = S\,\mu_{(l)}\,l^3\,\nu^2\,k'$$

which acts in the plane of rotation or the propeller disk.

Hence, the closer the point of intersection lies to the k' axis the larger is the moment. This is seen with the aid of figure 36, where the F_S function is plotted for $\alpha = 0^\circ$ and $\alpha = 60^\circ$ and, furthermore, for $\alpha = 60^\circ$ for the case that the blade is hinge-connected about the chord and hence a moment on the shaft can be transmitted only over the smaller axis (dotted). In the figure are also given three engine curves, one of which represents the case that the natural frequency of the torsionally vibrating system is equal to the first harmonic of the blade about the small axis. This case will be considered first (curve II). For the angle $\alpha = 0$ the blade vibrates about the small axis in the torsional vibration plane of the hub. The moment in the hub is obtained as infinitely large. Since in the actual case there is damping a finite deflection will be obtained for the rod and the torsionally vibrating mass. Let the deflection of the mass be Φ_{D_0}. The intensity of the rod vibration on changing the angle α cannot increase, therefore, for the case of constant excitation. For any angle the natural frequency of the system does not vary, since the point of intersection which determines this frequency remains the same. There is also, therefore, no change in the mode of vibration of the rod about the small axis and the moment in the blade root. In the torsional vibration plane, however, a component of the moment is still effective and hence the balance moment of the torsionally vibrating mass $\theta_D \omega^2 \Phi_{D_\alpha}$ must decrease. Since θ_D and ω are constant

$$\Phi_{D_\alpha} = \Phi_{D_0} \cos \alpha$$

The case is otherwise for engine curve I. With the blade hinged about the chord there is a change not only in the frequency and hence the mode of vibration of the blade but also the distance of the new point of intersection from the k' axis is greater and the moment therefore smaller (fig. 37). The deflection Φ_D of the torsionally vibrating mass therefore decreases faster than as $\cos \alpha$. In this case the angular deflection at the hub is not equal to zero. From equation (4) there follows the relation

$$\Phi_D = \Phi_N \frac{1}{1 - \frac{\omega^2}{\Omega^2}}$$

so that for the angle $\alpha = 0$

$$\Phi_{D_o} = \Phi_{N_o} \frac{1}{1 - \frac{\omega_o^2}{\Omega^2}}$$

and for the angle α

$$\Phi_{D_\alpha} = \Phi_{N_\alpha} \frac{1}{1 - \frac{\omega_\alpha^2}{\Omega^2}}$$

or

$$\Phi_{D_\alpha} = \Phi_{D_o} \frac{\Omega^2 - \omega_o^2}{\Omega^2 - \omega_\alpha^2} \frac{\Phi_{N_\alpha}}{\Phi_{N_o}}$$

The ratio $\Phi_{N_\alpha}/\Phi_{N_o}$ is a function of α. It may be determined as follows. The formula must also hold if ω_o approaches Ω - that is, for the case first considered. For that case there was obtained

$$\Phi_{D_\alpha} = \Phi_{D_o} \cos \alpha$$

The fraction

$$\frac{\Omega^2 - \omega_o^2}{\Omega^2 - \omega_\alpha^2}$$

approaches 1, if ω_o approaches Ω. It follows that $\Phi_{N_\alpha}/\Phi_{N_o}$ approaches cos α. As may be seen from figure 36, the moment in the hub in the case of fixed end conditions decreases still more than for hinged end conditions. This not only shows up in the expression for Φ_{D_α} by the decrease in the fraction but also in the fact that the ratio $\Phi_{N_\alpha}/\Phi_{N_o}$ always remains below cos α. The reason for this was already given above. The more $y'^h_{(l)}$ falls in the torsional vibration plane the smaller Φ_{N_α} must become (fig. 38). The angular deflection Φ_N of the hub thus decreases more rapidly than as cos α, and hence Φ_D further decreases.

Figures 39, 40, and 41 show the variation of the angular deflection of the rotating mass of a single-mass system for the case of the rectangular section rod and for the propeller. The analogy of the propeller and rod is clearly evident as already seen in figure 19. A comparison with the latter shows that for the cases where the frequency was constant or approximately so, with change in the angle α, the angular deflection of the rotating mass decreased in proportion to $\cos \alpha$. In all other cases the deflection decreases at a greater rate. The indicated angle is only a relative one in order to bring out better the analogy with the rectangular rod. The greatest absolute deflection of the rotating mass measured in the center was obtained at an angle of approximately 15° for the fundamental vibration, 0° for the first harmonic and 30° for the second harmonic.

It should be observed that the above described dependence of the deflection Φ_N on the angle α holds only for cases represented by engine curves I and II. For cases represented by curve III this holds true only for the fundamental vibration, but not for the torsional vibration and first harmonic. For $\alpha = 0$ there is then obtained a greater first harmonic about the small axis and the second node lies in the blade and not in the blade root. With increase in the angle α this vibration goes over into the torsional vibration, while it is still represented by the point of intersection of engine curve III with the second branch of the $F_S(k')$ curve. In the case, therefore, that the torsional vibration is on the opposed side of the first harmonic, like the fundamental vibration of the blade fixed at one end about the chord, the moment at the hub in the torsional vibration plane decreases somewhat with decrease in the angle α but the angular deflection Φ_D of the rotating mass and hence also the moment transmitted by it to the rod, need not decrease because the motion of the hub can increase through the increase of $y'^{f\zeta}_{(\zeta)}$ in Φ_N. This is the case for the torsional vibrations represented in figure 20 by engine function III and on figure 21 by engine function I.

For the first harmonic in the case of engine function III Φ_D is small although the dependence shown in figure 38 of the hub deflection on the angle α no longer

applies because it decreases with further decrease in α. The intersected $F_S(k')$ curve then deforms into straight lines and the point of intersection travels further up until for $\alpha = 0$ this branch of the $F_S(k')$ curve, and hence also the vibration, has entirely vanished.

The previous considerations have shown in which cases large and small deflections of the rotating mass occur. In spite of small deflections the stress in the propeller blade about the chord may be considerable even for small $y\left(\frac{b}{l}\right)$, and the torsiogram on account of the small motion of the rotating mass would not reveal these dangerous stresses. Since the torsional vibration system and particularly the propeller blades vibrate only with damping, energy must be expended by the exciting torque. In consequence, the magnitude of the moment M_E as well as the the angle ζ, where $M_E \zeta$ is the excitation work, are involved. In the case of the airplane engine and its equivalent single-mass system the excitation is on the rotating mass, $\zeta = \Phi_D$. For equal frequency, therefore, all propeller vibrations will be excited with less intensity the further the point of intersection of the $F_M(k')$ and $F_S(k')$ curves is from the k' axis. The stressing of the propeller blade will therefore also become smaller. From these considerations it follows that the fundamental vibration may be considered less dangerous as compared with the torsional vibration and the first harmonic because conditions in practice are such as represented in figures 20 and 21.

If still higher than the first harmonic vibrations are considered, it is seen that their point of intersection will always lie below the k' axis, provided the mass of the hub is small enough so that the frequency

$$\omega = \sqrt{c \frac{\theta_D + \theta_N}{\theta_D \theta_N}}$$

is greater than the harmonic under consideration. Since the rotating mass deflection for vibrations the corresponding point of intersection of which lies far below the k' axis is given by the relation

$$\Phi_D \approx \frac{\theta_N}{\theta_D} \Phi_N$$

this is favorable. For the higher harmonics a large hub mass is less favorable since, as comparison of figures 17 and 18 shows, their corresponding points of intersection again lie near the k' axis. There is thus an increase in the moment at the hub which in spite of the small angular displacement can be balanced by the inertia of the large hub mass.

Since the rod or propeller blade divides the moment at the hub into two bending moment components in the principal vibration directions, that vibration will predominate about each axis having zero position $F_S(k') = 0$ nearest to the point of intersection of $F_S(k')$ and $F_M(k')$, giving the resonance position. Hence, if the torsional vibration lies in the neighborhood of the first harmonic the latter will come into evidence. This is the reason why the mode of vibration of the propeller, as initially remarked for the torsional natural vibration of the test model (col. 2, table 1), was similar to that of the first harmonic (col. 3) since, chiefly, the larger motions on account of the small equatorial moment of inertia are in evidence. In this case for both vibrations the mode of vibration about the small axis is very marked and the blade tip failures that sometimes occur in wood propellers may, judging by the failure location, be caused by the first harmonic as well as by the torsional vibration. The more closely together the frequencies lie the greater is the moment due one of the vibration modes that must be added to the other decreasing vibration. The maximum value of the moment M_D as a function of the angular setting is then obtained, neglecting the twist of the blade, not at the angle $\alpha = 90^\circ$ but for $\alpha = 90 - \epsilon$ where the tangent of this angle is given by the ratio of the two perpendicular components of the moment (fig. 42).

The components of this moment were computed for the prismatic homogeneous rod for the undamped case from the function $F_S(k')$ and the results plotted in figure 43, the ratios of the components M_h and M_{fl} to the moment at the hub M_D being plotted against k' for an angle $\alpha = 60^\circ$ with $J_h/J_{fl} = 16$ and $r = 0$.

At the asymptotic positions the torsional moment at the hub M_D is equal to zero. It may be seen from the curves that except for the very small regions about the resonance positions of the vibrations about the small

axis for $k_e' = 1.875$; 4.694, and so forth; the moment in the shaft is entirely balanced by vibrations about the chord. This means in practice that the propeller blade behaves quite similarly so that in the torsional vibration the maximum moment that arises is almost entirely in the direction of the larger axis. This explains the position of the failure (fig. 44). The setting for the cross section at the blade root is about 40°. Since only the sine component acts on the torsional vibration system, only 64 percent of the moment actually arising at the blade root is computed from the torsiograph deflection.

B. Tests

In order to obtain a clear picture of the relations so far considered, mostly from the theoretical viewpoint, in determining the $F_S(k')$ function of the deflections of the Ju PAK propeller (fig. 29); the rotating mass and hub were measured with the aid of an attached mirror which threw an image of an illuminated slot on a screen. For this measurement, however, only cases c to g can be considered because only for these cases was the rotating mass of the same magnitude as is necessary for a proper comparison. In addition the blade tip deflections of the Ju PAK propeller were directly measured. Under the heading A_{Ob} in table 3, 10/18, for example, denotes that the first number is the deflection of the rotating mass on the screen in centimeters the other the deflection of the blade tip in millimeters, both being for the first harmonic. A_D gives the deflection for the torsional vibration. The angular deflections of the hub were in all cases negligibly small compared to those of the rotating mass and were therefore not entered. Besides the cases denoted with the letters which are given in figure 29, a few further cases were considered in order that the continuous change in the relations could be more readily seen. For greater clarity they were not plotted. Since the comparison of the deflections must be carried out for equal excitation while the unbalance excitation increases as the square of the speed, all deflections are referred to the excitation for a definite speed. The latter was chosen as 7300 rpm, corresponding to $k_e' = 3.3$.

From the discussion under section Solution for the Homogeneous Rod, the torsional vibration frequency for

cases a to e lies below and for cases f to k above the first harmonic. Since it must be concluded from this that there is a sudden jump from the torsional vibration to the first harmonic and, conversely, there will first be explained in what sense in cases e and f an interchange of the torsional vibration with the first harmonic is to be understood. This jump is determined only by the condition that each vibration form has been defined by means of certain physical properties.

In table 3, the first column, the frequencies and deflections of c to g are those which correspond to the intersection of the various $F_M(k')$ curves with the $F_S(k')$ branch, which extends from $k' = 2.06$ to 3.3. The frequency runs from $n = 5580$ to the limiting value of 7300 rpm.

The change in the deflections is entirely continuout. The case e' which was not plotted corresponds to the case that an $F_M(k')$ curve goes accurately through the point of intersection of the $F_S(k')$ curve with the k' axis at $k_e' = 3.3$; f' is a closely neighboring case which likewise has not been plotted.

The second column of the frequencies and deflections includes those which correspond to the points of intersection of the $F_M(k')$ curves with the $F_S(k')$ branch which extends from $k' = 3.3$ to 4.33.

Thus, in all cases which correspond to the same $F_S(k')$ branch, the variation of the deflections with the frequency is continuous and such a branch gives both the torsional vibration and any harmonic of the propeller. Both branches and their corresponding vibrations are, so to speak, equivalent. It may be considered that one branch transfers the torsional vibration to another if the latter can give rise to a similar vibration. This is only possible where an $F_M(k')$ curve intersects the two $F_S(k')$ branches in such a manner that the two vibrations lie most closely together. Case e' therefore represents the limit for which, according to the discussion under section Solution for the Homogeneous Rod, it is still possible to speak of the higher natural frequency of the system as the first harmonic.

For the individual modes of vibration the following result is obtained. With the deflections of the rotating mass known, the first harmonic provides a measure of the magnitude of the moment at the hub; since $M_D = \theta_D \omega^2 A_{Ob}$ for constant θ_D and practically constant ω depends only on the deflection A_{Ob}. It may be seen that the magnitude of the deflection decreases with increasing distance of the point of intersection of the $F_M(k')$ curve with the $F_S(k')$ curve from the k' axis, in agreement with the theory, and furthermore that the blade tip deflections themselves, and hence also the stresses in the blade, decrease. That the deflections for the vibrations, the point of intersection of which lies above the k' axis with increasing distance of the latter, decrease more rapidly than for those the point of intersection of which lies below the axis, is explained by the presence of a mass moment of inertia of the hub that is not negligible in comparison with that of the rotating mass; and by the fact that in the first case with increasing distance of the point of intersection from the k' axis the shaft became more rigid while in the second case less rigid. For two points of intersection at equal distance above and below the k' axis, there then holds the relation

$$\Phi_{D_2} = \Phi_{D_1} \frac{\theta_D + \theta_N \left(1 - \frac{\omega^2}{\Omega_1^2}\right)}{\theta_D + \theta_N \left(1 - \frac{\omega^2}{\Omega_2^2}\right)}$$

where

$$\frac{\omega^2}{\Omega_1^2} < 1 \quad \text{and} \quad \frac{\omega^2}{\Omega_2^2} > 1$$

From this relation it follows that the deflections of the rotating mass become equal when $\theta_N = 0$. All this can also be understood from the fact that in the first case the hub vibrates with the rotating mass and in the second case against it. In both cases, however, there corresponds to a given rotating mass deflection approximately the same blade tip deflection, since the mode of vibration of the rod must be approximately the same.

In the torsional vibration the deflections can no longer serve as a measure for the moment, because the frequency continuously changes. Consideration of the ratio of the blade tip deflection to that of the rotating mass shows, however, that on approaching the first harmonic the latter comes more into evidence so that the torsional vibration in case e' corresponds approximately to the first harmonic in case f' and conversely.

Another important fact obtained from the experiment is that for propellers of the Ju PAK type where the fundamental vibration of the blades about the chord 1 is lower than the first harmonic about the small axis the blade vibrations set up about the small axis are relatively large if the torsional vibration lies below the first harmonic and small if it lies above the latter.

Setting up the same table for an untwisted prismatic rod, the same general results are obtained except for the condition that the rod, with regard to the above-mentioned property of the propeller, behaves in just the reverse manner provided that for the rod under consideration; the fundamental vibration about the chord likewise lies lower than the first harmonic about the small axis. Further investigations on this question revealed a fundamental difference between rod and propeller blade. On observing the direction of vibration of the propeller tips it was found that as the torsional vibration approaches the first harmonic the direction rotates in both cases, and that this occurs in the rod in exactly the opposite sense to that in the propeller blade. Figure 45 shows this turning of the vibration direction of the propeller blade tip. From this direction of vibration the corresponding vibration modes of the blade can be immediately derived. This is shown in figure 46. For each case the vibration mode about the small axis (dotted) and that about the chord (continuous) are drawn as projections in the torsional vibration or propeller disk plane.

In the case $k' < 3.3$ the vibration moment of the two vibrations has the same direction; for $k' = 3.3$ there is practically no vibration about the chord; and for $k' > 3.3$ the moments about the chord and small axis act in opposite directions.

For the prismatic untwisted rod the theory requires a rotation of the direction of vibration as shown in figure 47. For the vibration modes are obtained from these

directions such that the components of their moments at the blade roots in the torsional vibration plane have the combined effect shown in figure 43, as was also observed. The same behavior is observed with a prismatic nonhomogeneous rod with constant thickness and width decreasing toward the outer end ($x = 0$) so that the particular behavior of the propeller blade should be determined by the twist. Further investigations will throw more light on this. In the same way both stroboscopic observations of the vibration phenomenon and the observed elliptic paths of each point of the propeller blade indicate a phase shift of the vibration about the chord with respect to that about the small axis.

The difference in the magnitude of the deflections of the rod and blade tips, respectively, about the small axis for the torsional vibration above the first harmonic compared to those below is thus explained. Quite generally, it is true that the motion about the small axis in the torsional vibration is then relatively large if the moment of the vibration mode about the small axis acts in the same sense as that about the chord (see fig. 43).

The results here obtained now make it possible, in the case of propellers of the Ju PAK types, to state the approximate direction in which the resultant maximum vibration moment acts in the blade root during torsional vibration if the latter falls very closely above or below the first harmonic. The thin arrows in figure 48 give the direction of the moment about both axes for the vibrations corresponding to $k' = 2.97$ and 3.3 – that is M_h and $M_{f\zeta}$.

The quantitative solution of these problems and determination of the location of the maximum stress for the various vibration modes of the system, which requires many tedious strain measurements since the vibrations depend to a large extent on the cross-section shape, will form the subject of a future investigation of the institute.

For both vibrations corresponding to the value $k' = 2.97$ and 3.3, the torsionally vibrating system vibrates in resonance $\omega = \Omega$. For $k' = 2.97$ the vibrations about the small axis are a minimum, and the fundamental vibration of the blade is about the chord. At $k' = 3.3$ the vibration about the chord is a minimum and the first harmonic is about the small axis.

In order to show the difference between a flight propeller and a rigid propeller, a heavy rigid iron plate of moment of inertia $\theta_L = 64$ kgcms^2 was attached to the shaft instead of the propeller and the deflection of the rotating mass was measured for equal resonance frequency. This means that instead of the propeller function any other engine function intersects so that the point of intersection lies directly on the k' axis. The values obtained were

k'	A_D	A'_D	V
2.97	35	45	1.29
3.3	10	29	2.90

A'_D is the deflection with the plate and V is the ratio of the two deflections. Since in both cases the frequency was the same, V at the same time gives the ratio of the moments in the shaft.

The above is an explanation of the fact that in the torsiogram the deflections with the flight propeller are generally smaller than those with a rigid brake propeller, since the lowest natural frequency of the brake propeller lies higher than that of the torsional vibration system - that is, $\Omega < \frac{2\pi}{60} n_1$. These cases are represented in the F_S, F_M diagrams if the F_M function intersects the k' axis to the left of the corresponding k' value; for the homogeneous rod k' = 1.875. Comparison of figures 5 to 15 shows that the resonance frequencies so defined are practically independent of the pitch angle. The resultant falls practically in the torsional vibration plane so that on the entire brake propeller there is no greater moment than that computed from the torsiodiagram, because the $F_S(k')$ curves for $\alpha = 0$ and 90° run practically the same within the range considered. In this case $M_{fl(\alpha=0)} \quad M_{h(\alpha=90^\circ)}$ and hence for any angle α

$$M^{fl}_{(\alpha=0)} \cos^2 \alpha + M^{h}_{(\alpha=90^\circ)} \sin^2 \alpha \approx M_D = \text{constant}$$

Translation by S. Reiss,
National Advisory Committee
for Aeronautics.

REFERENCES

1. Southwell: Graphical Method for Determination of the Frequencies of Lateral Vibrations. Phil. Mag., vol. 41, 1921.

2. Southwell, R. V., and Gough, Barbara S.: On the Free Transverse Vibrations of Airscrew Blades. R. & M. No. 766, British A.R.C., 1922.

3. Liebers, F.: Contribution to the Theory of Propeller Vibrations. T.M. No. 568, NACA, 1930.

4. Liebers, Fritz: Resonance Vibrations of Aircraft Propellers. T.M. No. 657, NACA, 1932.

5. Hohenemser, K.: The Dynamics of the Elastic Bar as Applied to the Propeller. (Trans.)* Z.F.M., vol. 23, no. 2, Jan. 28, 1932, pp. 37-43.

6. Liebers, Fritz: Propeller Tip Flutter. T.M. No. 683, NACA, 1932.

7. Hansen, M., and Mesmer, C.: Luftschraubenschwingungen. Z.F.M., vol. 24, no. 11, June 6, 1933, pp. 298-304. Airscrew Oscillations. Airc. Engineering, vol. 7, no. 73, March 1935, pp. 65-69.

8. Reissner, H.: Formänderung, Spannung und kleine Schwingungen von Stäben mit anfänglicher Krümmung und Verwindung, die um eine Querachse rotieren. Ing.-Archiv., Bd. 4, 1933.

9. Morris, J.: Some Dynamical Characteristics of Propellers. Jour. R.A.S., vol. 38, no. 288, Dec. 1934, pp. 987-997.

10. Caldwell, W.: Aircraft-Propeller Development and Testing Summarized. SAE Jour., vol. 35, no. 2, Aug. 1934, pp. 297-310 and no. 3, Sept. 1934, pp. 349-353.

11. Couch, H. H.: A Study of Propeller Vibration. Aviation, vol. 33, no. 6, June 1934, pp. 179-180.

*Available for reference or loan in the Office of Aeronautical Intelligence, National Advisory Committee for Aeronautics.

12. Liebers, F.: Analysis of the Three Lowest Bending Frequencies of a Rotating Propeller. T.M. No. 783, NACA, 1936.

13. Riz, P.: The Resonance Method of Determination of the Natural Frequency of Airscrew Blades. CAHI No. 242, 1935. (Russian)

14. Theodorsen, T.: Propeller Vibrations and the Effect of the Centrifugal Force. T.N. No. 516, NACA, 1935.

15. Ramberg, Walter, Ballif, Paul S., and West, Mack J.: A Method for Determining Stresses in a Nonrotating Propeller Blade Vibrating with a Natural Frequency. Nat. Bur. of Standards Jour. Res., vol. 14, no. 2, Feb. 1935, pp. 189–215.

16. Munk, Max M.: Propeller Forces. And a Suggested Correction Factor for Use in Their Calculation. Aero Digest, vol. 26, no. 5, May 1935, pp. 22, 24, 26.

17. Lürenbaum, K.: Schwingungen des Systems Kurbelwelle–Luftschraube. Luftfahrtforschung, Bd. 13, Lfg. 10, Oct. 12, 1936, pp. 346–356 and DVL Jahrb. 1937, pp. II 117–127. Vibration of Crankshaft Propeller Systems. SAE Jour., vol. 39, no. 6, Dec. 1936, pp. 469–479.

18. Couch H. H.: Propeller–Crankshaft Vibration Problems. Trans. Mech. Engineers, vol. 58, no. 4, Apr. 1936, pp. 215–21.

19. Carter, B. C.: The Vibration of Airscrew Blades with Particular Reference to Their Response to Harmonic Torque Impulses in the Drive. R. & M. No. 1758, British, A.R.C., 1937.

TABLE 1.- NATURAL VIBRATION OF A SINGLE-MASS SYSTEM WITH DIFFERENT PROPELLERS

Propeller	n_1	n_D	n_2
1. Schwarz, adjustable 3-blade, for He 111; D = 3308 mm	3000	6800	7600
2. Schwarz, adjustable for SAM 323 He 50; D = 3650 mm	2500	6300	5700
3. Schwarz, adjustable club for SAM 323 D = 2160 mm	4800	6600	9000
4. Schäfer As-10; D = 2500 mm	2950	6600	9300
5. Ju PC	2000	6400	5500
6. 3-blade VDM adjustable dural for Do 17	2700	6700	8800
7. 2-blade VDM adjustable	2200	5800	6900
8. Heine, wood; D = 2270 mm	3060	6300	9500

TABLE 2

$F_M(k')$	θ_D kgcms^2	Ω^2 s^{-2}
a	15.0	113,000
b	9.33	209,000
c	4.93	345,000
d	4.93	417,000
e	4.93	528,000
f	4.93	720,000
g	4.93	1,130,000
h	3.3	1,690,000
i	2.4	2,320,000
k	2.4	3,530,000

TABLE 3

$F_M(k')$	n_D	A_D	n_{Ob}	A_{Ob}
c	5580	57/14	7300	1/10
	5880	54/13	7300	1.3/13
d	6150	45/14	7300	2/14
	6450	36/22	7300	2.5/16
e	6830	27/27	7300	4.5/18
	7020	23/30	7300	7/19
e'	7100	16/32	7300	10/18

$F_M(k')$	n_{Ob}	A_{Ob}	n_D	A_D
f'	7170	10/28	7380	14/17
	7230	6/20	7500	13/9
	7300	3/17	7700	12/5
f	7300	2/15	7930	11/2
	7300	1/10	8550	9/0.7
g	7300	0.5/9	9600	6/0.6

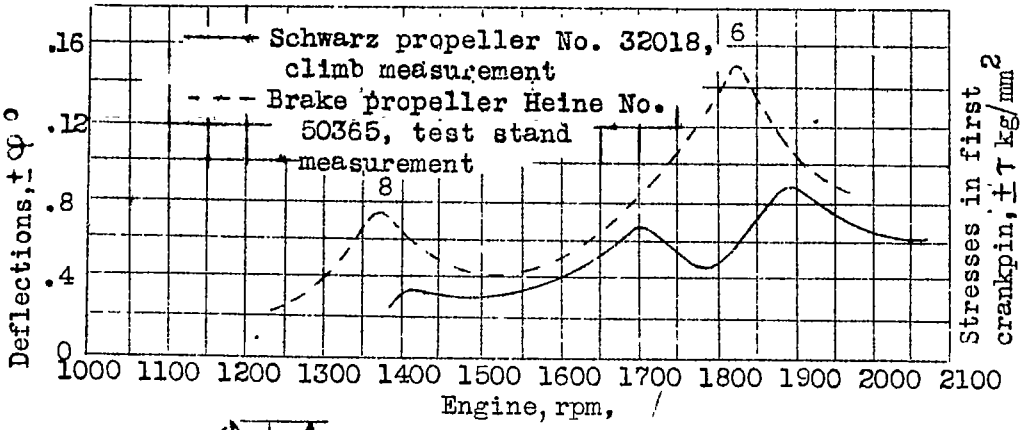

Figure 1.- Torsional vibration characteristic of a 4-cylinder in-line engine as measured on test stand and in flight.

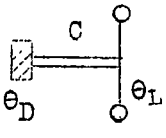

Figure 3.- Equivalent system of radial engine with rigid propeller.

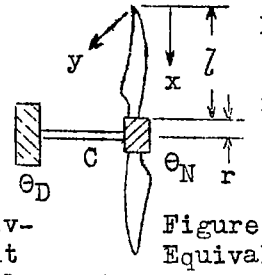

Figure 4.- Equivalent system of radial engine with elastic propeller.

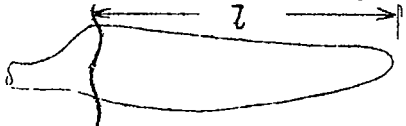

Figure 28.- Blade length l for the experimental determination of the propeller function $F_s(k')$.

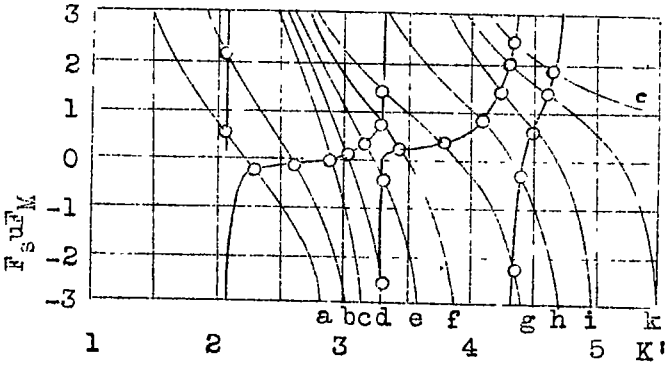

Figure 29.- Determination of the $F_s(k')$ function of a Ju PAK : adjustable propeller.

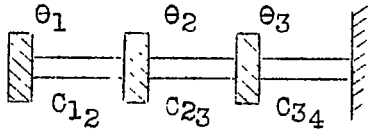

Figure 30.- Rotating mass system.

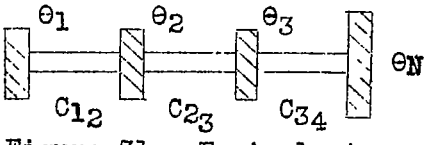

Figure 31.- Equivalent system of in-line engine with propeller hub.

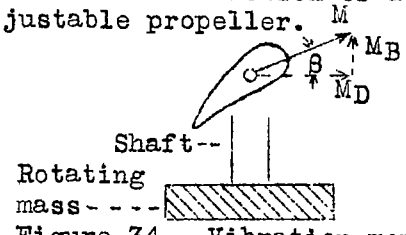

Figure 34.- Vibration moment in the propeller blade.

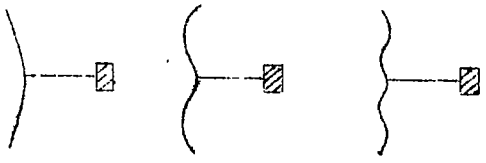

Fundamental vibration | First harmonic | Second harmonic

Figure 35.- Natural vibration modes of the propeller on engine.

Figure 2.- Exciter apparatus for coupling vibrations of crankshaft-propeller system.

Figure 16.- Vibration tests with prismatic homogeneous rod for varying pitch setting.

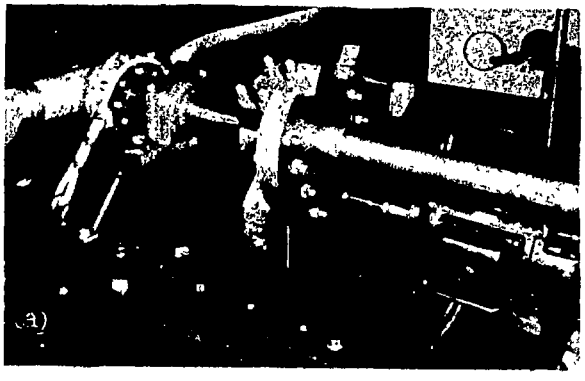

Figure 27.- Exciter apparatus for propeller vibrations with variable torsional elasticity and rotating mass to approach the actual engine conditions.

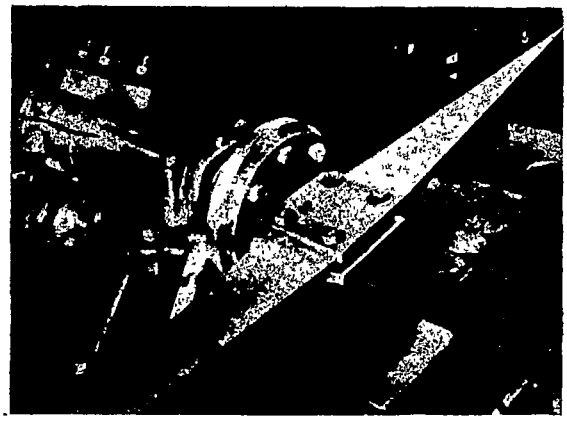

Figure 26.- Vibration tests with a non-homogeneous rod.

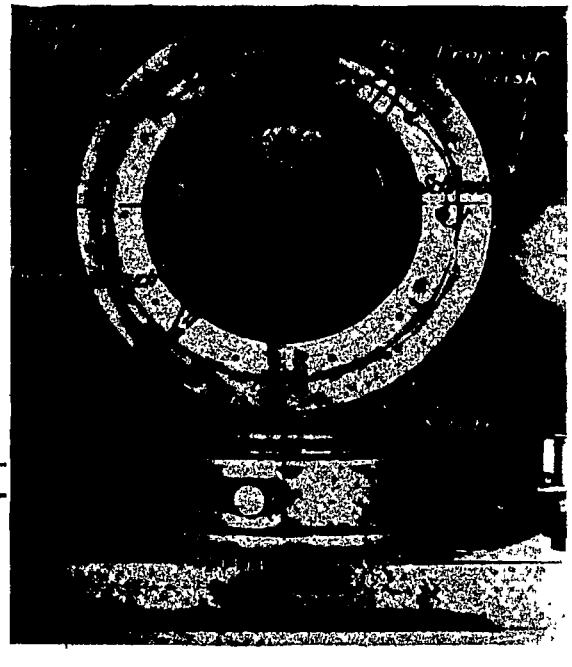

Figure 44.- Failure due to flexural vibrations of a light metal propeller at the blade root.

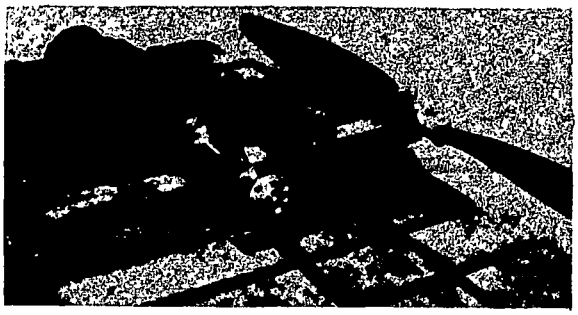

Figure 2.- Exciter apparatus for coupling vibrations of crankshaft-propeller system.

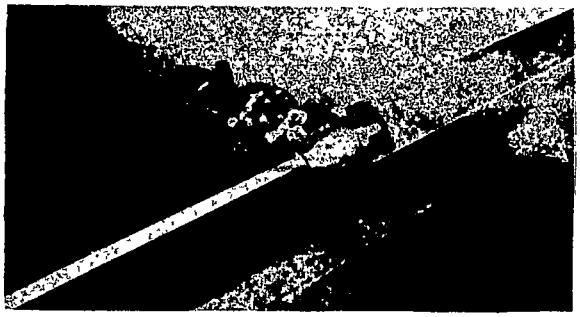

Figure 16.- Vibration tests with prismatic homogeneous rod for varying pitch setting.

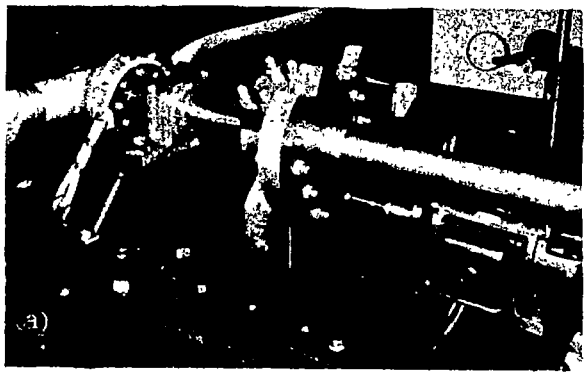

Figure 27.- Exciter apparatus for propeller vibrations with variable torsional elasticity and rotating mass to approach the actual engine conditions.

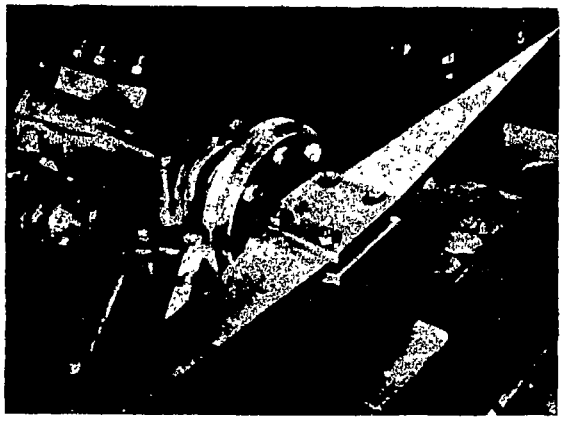

Figure 26.- Vibration tests with a non-homogeneous rod.

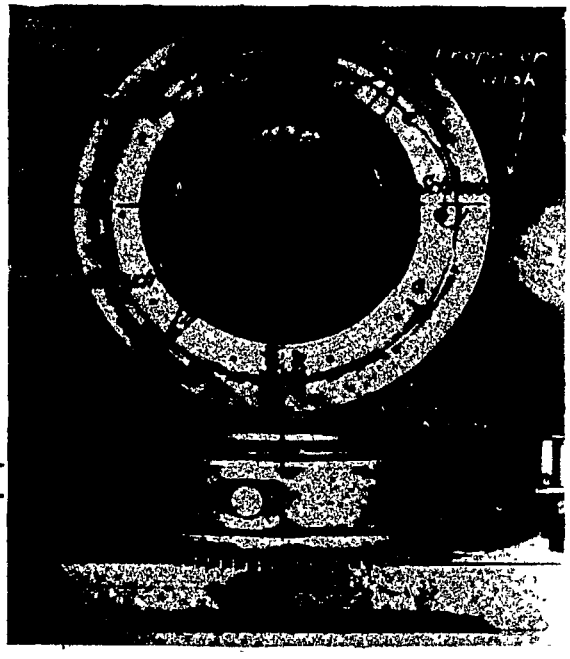

Figure 44.- Failure due to flexural vibrations of a light metal propeller at the blade root.

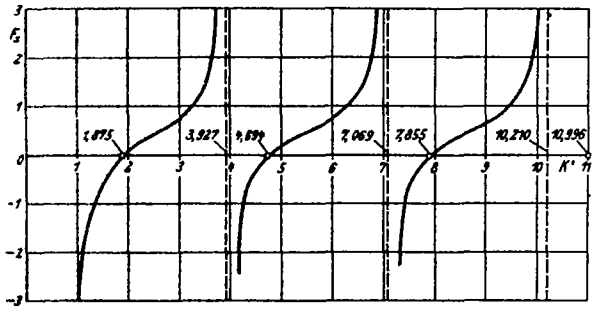

Figure 5.- Rod function of prismatic homogeneous rod. r = 0; α = 0.

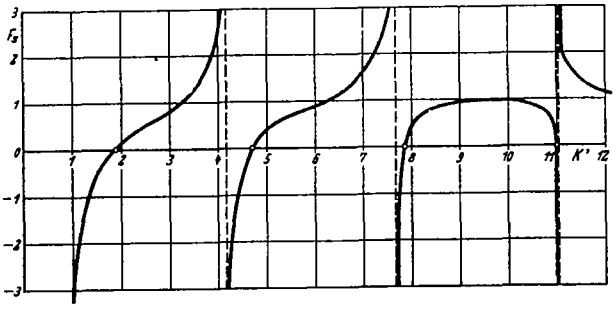

Figure 6.- Rod function of prismatic homogeneous rod. r = 0.1l; α = 0.

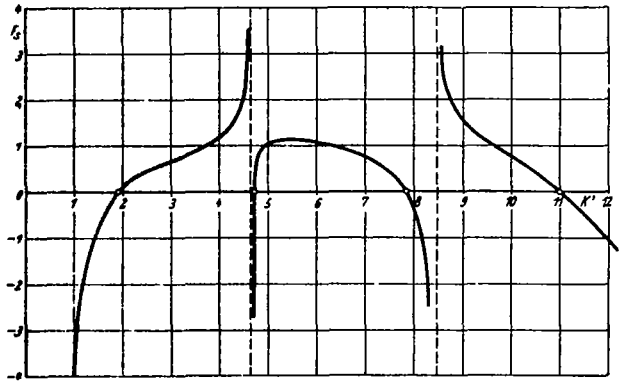

Figure 7.- Rod function of prismatic homogeneous rod. r = 0.2l; α = 0.

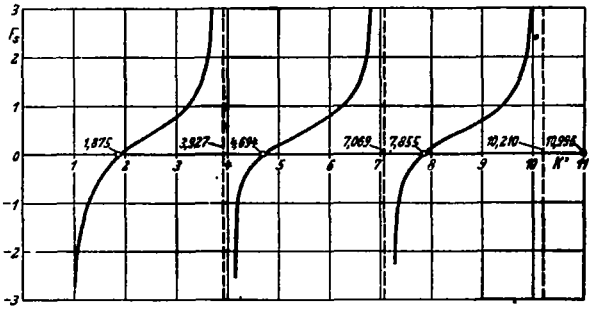

Figure 8.- Rod function of prismatic homogeneous rod. r = 0; α = 0; J_h/J_{fl} = 16.

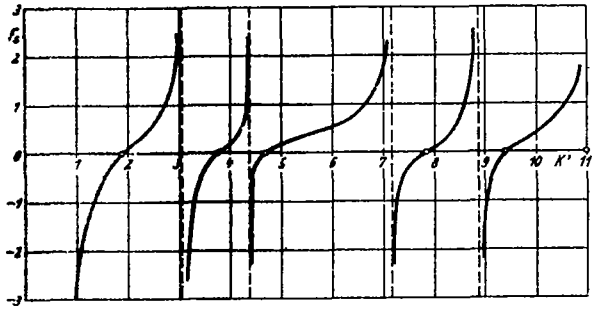

Figure 9.- Rod function of prismatic homogeneous rod. r = 0; $\alpha = 15^{\circ}$; J_h/J_{fl} = 16.

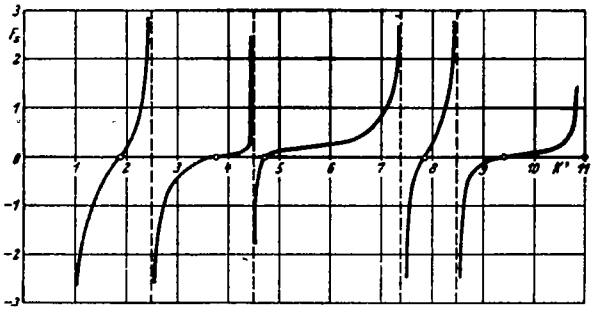

Figure 10.- Rod function of prismatic homogeneous rod. r = 0; $\alpha = 30^\circ$; $J_h/J_{fl} = 16$.

Figure 11.- Rod function of prismatic homogeneous rod. r = 0; $\alpha = 45^\circ$; $J_h/J_{fl} = 16$.

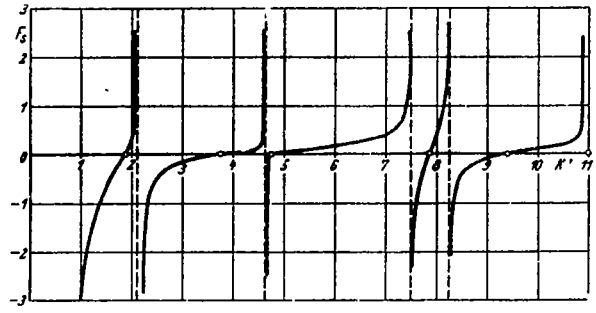

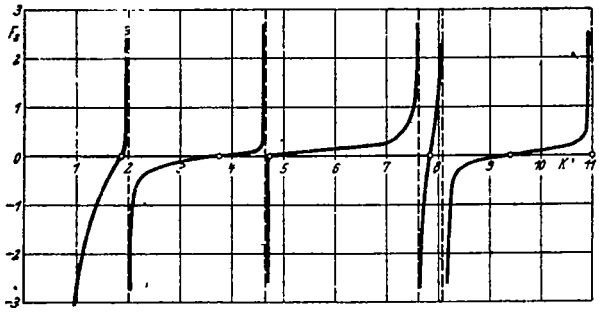

Figure 12.- Rod function of prismatic homogeneous rod. r = 0; $\alpha = 60^\circ$; $J_h/J_{fl} = 16$.

Figure 13.- Rod function of prismatic homogeneous rod. r = 0; $\alpha = 90^\circ$; $J_h/J_{fl} = 16$.

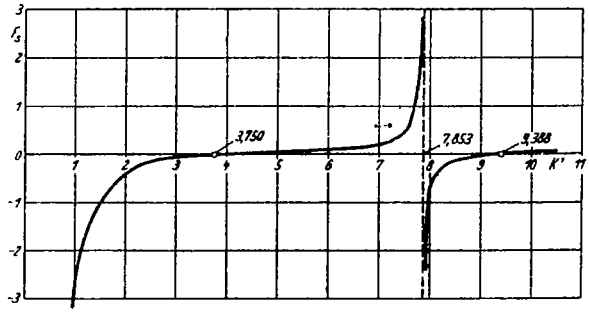

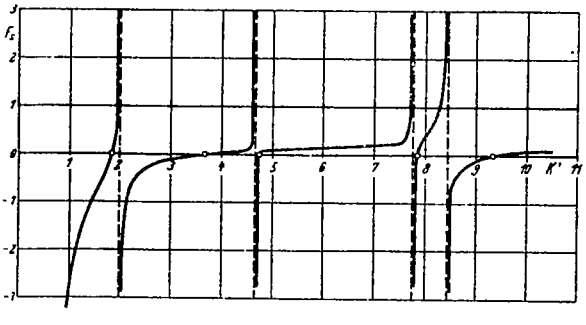

Figure 14.- Rod function of prismatic homogeneous rod. r = 0.1l ; $\alpha = 60^\circ$; $J_h/J_{fl} = 16$.

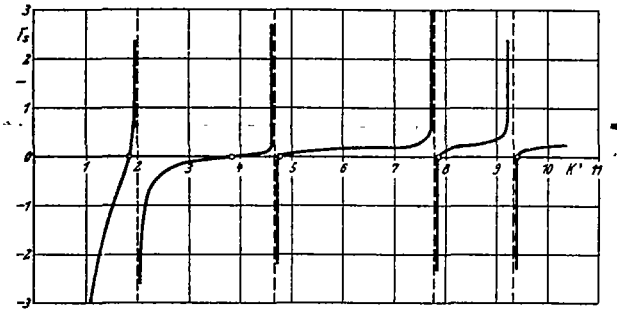

Figure 15.- Rod function of prismatic homogeneous rod. r = 0.2l; $\alpha = 60^{\circ}$; $J_h/J_{fl} = 16$.

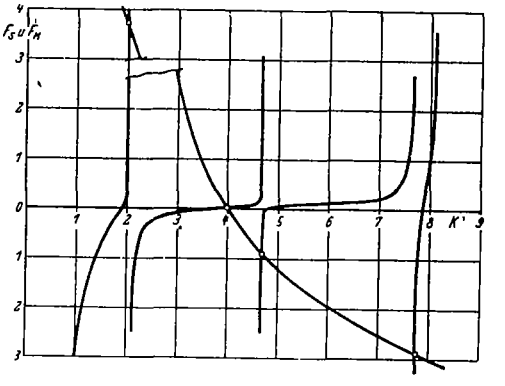

Figure 17.- Determination of the natural frequency of a single-mass torsionally vibrating system ($\theta_N = 0$) with two prismatic homogeneous rods. ($\alpha = 60^{\circ}$; r = 0).

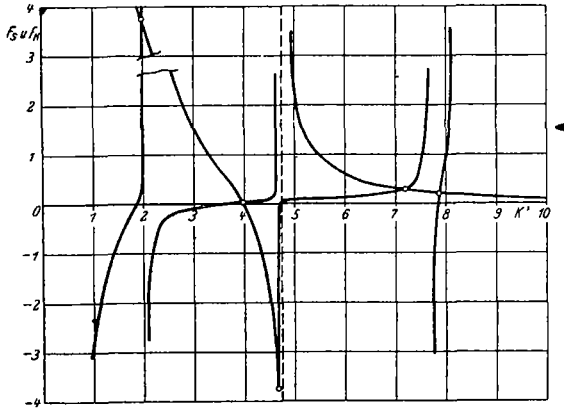

Figure 18.- Determination of the natural frequency of a single-mass torsionally vibrating system ($\theta_N = \theta_D$) with two prismatic homogeneous rods. ($\alpha = 60^{\circ}$; r = 0).

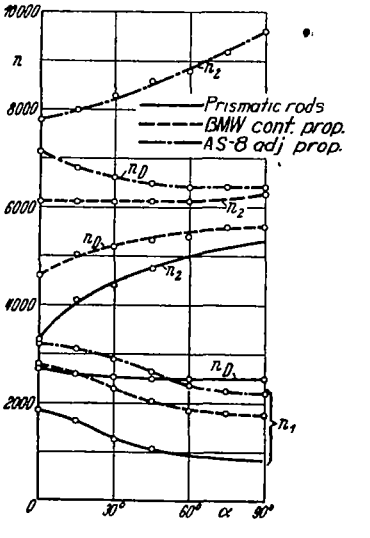

Figure 19.- Variation with the angle of the natural frequency of a single-mass torsionally vibrating system with two rectangular section rods (———), an AS-8 adjustable propeller (— - —), and a BMW controllable propeller (------), experimental.

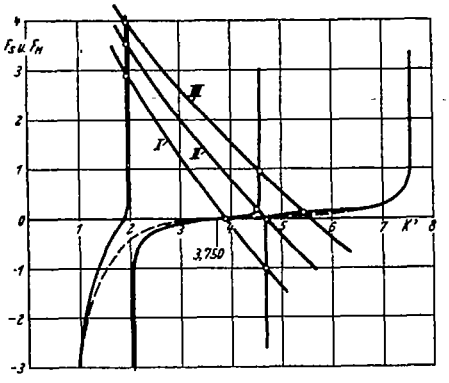

Figure 20.- Comparison of three different engine functions (α = 60°, r = 0, J_h/J_{fl} = 16).

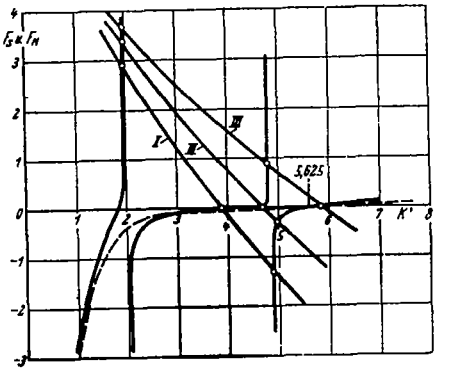

Figure 21.- Comparison of three different engine functions (α = 60°, r = 0, J_h/J_{fl} = 81).

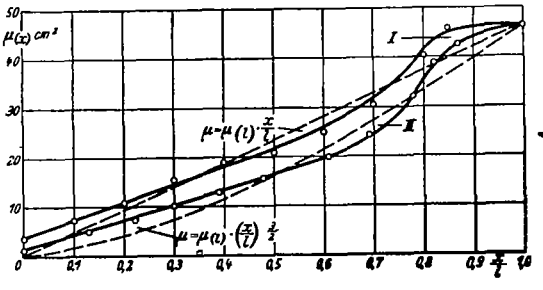

Figure 22.- Variation of $\mu(x)$ over the length of an AS-8 Elektron adjustable propeller (I) and an HM 8 u-Elektron adjustable propeller (II) (diameter 2.10 and 2.30 m).

Figure 23.- Variation of $J_{fl}(x)$ over the length of an AS-8 Elektron adjustable propeller (I) and an HM 8 u-Elektron adjustable propeller (II) (diameter 2.10 and 2.30 m).

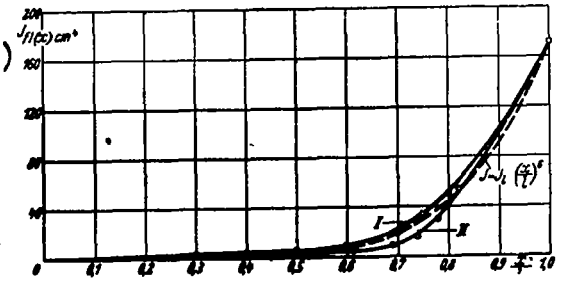

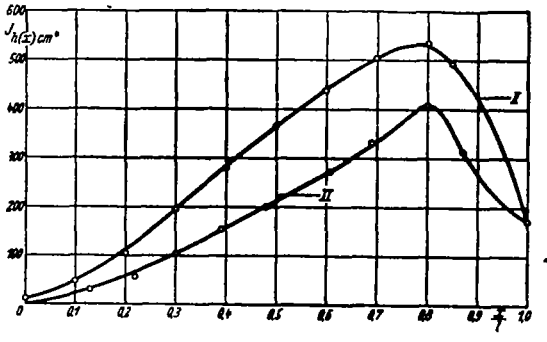

Figure 24.- Variation of $J_h(x)$ over the length of an AS-8 adjustable Elektron propeller (I) and a HM 8 u-Elektron adjustable propeller (II) (diameter 2.10 and 2.30 m).

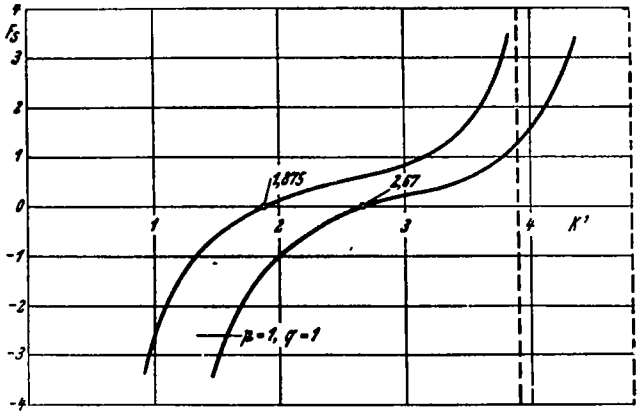

Figure 25.- Rod function for the fundamental vibration of the prismatic non-homogeneous rod (p = 1; q = 1) r = 0; α = 0.

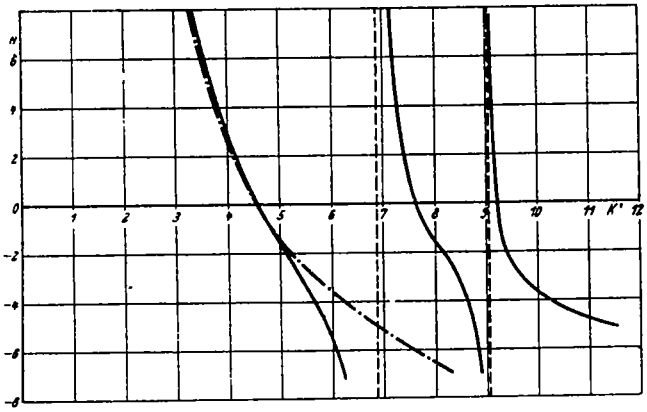

Figure 32.- Engine function (———) for three masses and the equivalent function (— · —) for one mass (θ_N = 0).

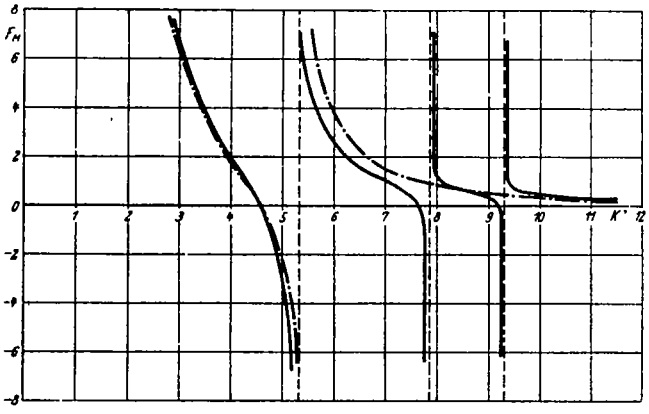

Figure 33.- Engine function (———) for three masses and the equivalent function (— - —) for one mass ($\theta_N = \theta_D$).

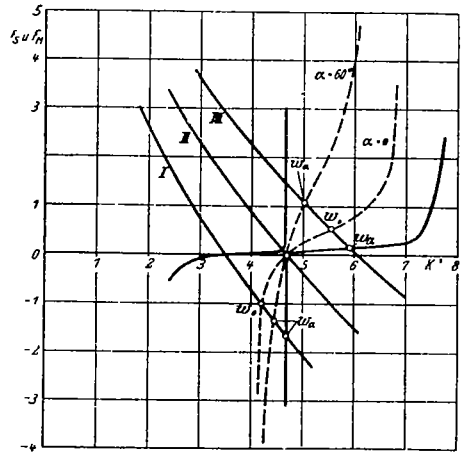

Figure 36.- Decrease in the moment by the vibration about the chord.

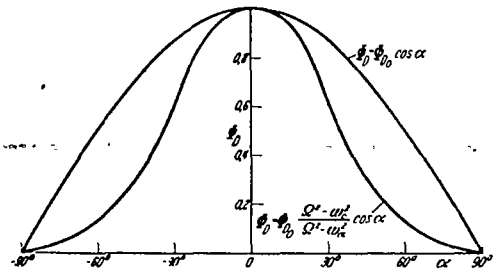

Figure 37.- Torsional vibration displacement of the rotating mass as a function of the angle α.

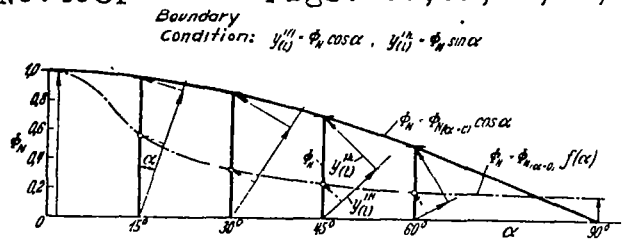

Figure 38.- Dependence of the angular displacement of the hub on the angle α.

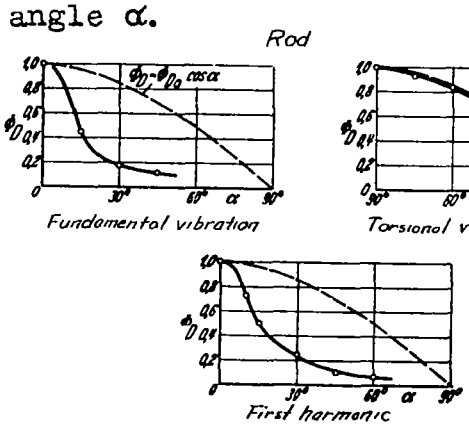

Figure 39.- Dependence of the rotating mass displacement Φ_D on the angle α for a rectangular iron rod for the fundamental vibration, torsional vibration, and first harmonic, experimental.

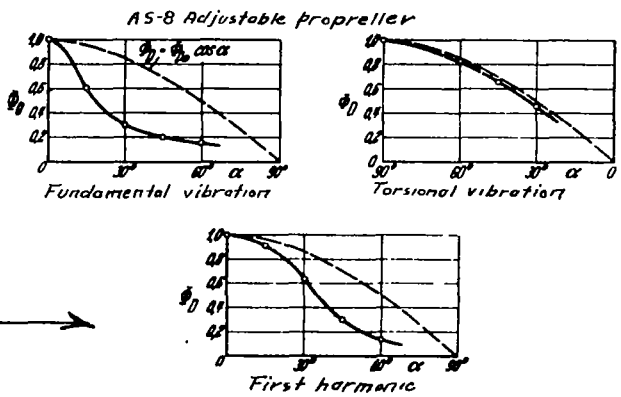

Figure 40.- Dependence of the rotating mass deflection Φ_D on the angle α for an AS-8 Elektron adjustable propeller for the fundamental vibration, torsional vibration, and first harmonic, experimental.

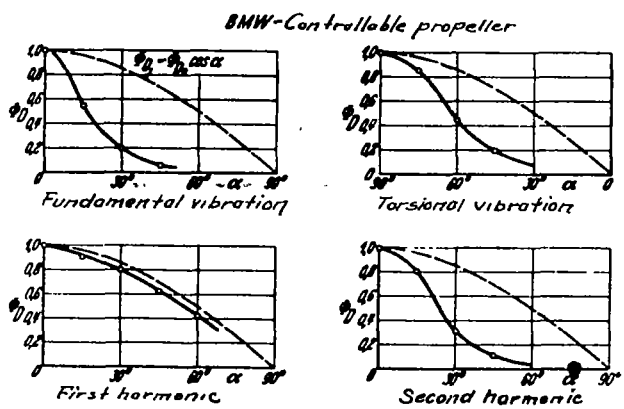

Figure 41.- Dependence of the rotating mass deflection Φ_D on the angle α for a BMW Elektron controllable propeller for the fundamental vibration, torsional vibration, first harmonic, second harmonic, experimental.

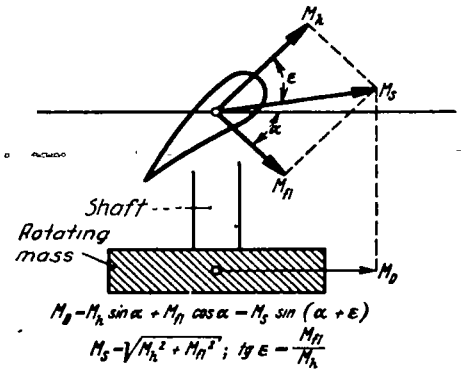

Figure 42.- Resolution of the vibration moment into the moments about the two principal axes of the cross section.

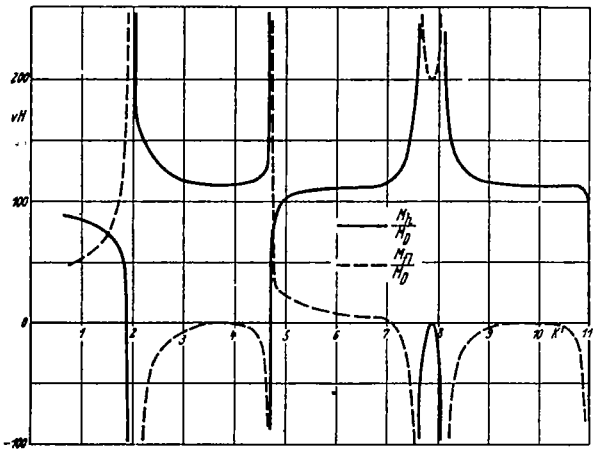

Figure 43.- Dependence of the ratios M_h/M_D and M_{fl}/M_D on k' for the prismatic homogeneous rod, computed for $\alpha = 60^\circ$, $r = 0$, $J_h/J_{fl} = 16$.

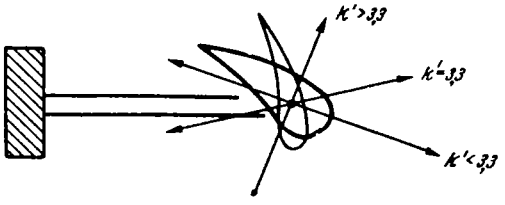

Figure 45.- Direction of vibration of the propeller tip for various values of k'

Figure 46.- Mode of vibration of propeller blade for various values of k'.

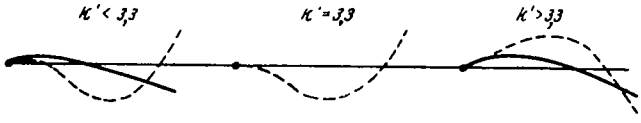

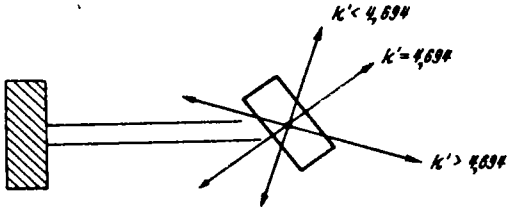

Figure 47.- Direction of vibration of tip of prismatic untwisted rod for various values of k'

Figure 48.- Direction of the maximum vibration moment at the propeller blade root for various torsional vibrations.